HOKKAIDO UNIVERSITY

Title	Incomplete Elongation of Ultra-long-chain Polyunsaturated Acyl-CoAs by the Fatty Acid Elongase ELOVL4 in Spinocerebellar Ataxia Type 34
Author(s)	Tamura, Yuka; Sassa, Takayuki; Nishizawa, Takumi et al.
Citation	Molecular and cellular biology, 43(2), 85-101 https://doi.org/10.1080/10985549.2023.2169563
Issue Date	2023-02-07
Doc URL	https://hdl.handle.net/2115/91300
Rights	This is an Accepted Manuscript of an article published by Taylor & Francis in Molecular and Cellular Biology on 07 Feb. 2023, available at: http://www.tandfonline.com/10.1080/10985549.2023.2169563.
Type	journal article
File Information	MCB00392-22R1_Merged_PDF.pdf

Hokkaido University Collection of Scholarly and Academic Papers : HUSCAP

Incomplete elongation of ultra-long-chain polyunsaturated acyl-CoAs by the fatty acid elongase ELOVL4 in spinocerebellar ataxia type 34

Yuka Tamura,[a] Takayuki Sassa,[a] Takumi Nishizawa,[a] Akio Kihara[a]

[a]Laboratory of Biochemistry, Faculty of Pharmaceutical Sciences, Hokkaido University, Sapporo, Japan

Running title: Pathogenesis of spinocerebellar ataxia type 34

Address correspondence to Takayuki Sassa (tasasa@pharm.hokudai.ac.jp) and Akio Kihara (kihara@pharm.hokudai.ac.jp)

ABSTRACT

Spinocerebellar ataxias (SCAs) are autosomal dominant diseases characterized by cerebellar atrophy and ataxia. The SCA subtype SCA34 is caused by specific mutations in the gene *ELOVL4*, which encodes a fatty acid (FA) elongase that synthesizes ultra-long-chain (ULC; ≥ C26) FAs. However, the pathogenesis and molecular mechanism that confers dominant inheritance remains unknown. Here, a cell-based assay demonstrated that each of the five known SCA34 mutants produced shorter ULC polyunsaturated FA-containing phosphatidylcholines (ULC-PCs) than wild-type protein, in the following order of severity: Q180P and T233M > W246G > I171T and L168F. Next, we generated knock-in mouse embryonic stem cells that contained heterozygous Q180P, heterozygous W246G, or homozygous W246G mutations. Neuronal differentiation-dependent production of ULC-PCs was reduced in heterozygous Q180P and homozygous W246G cells relative to control cells, and we observed shortening of the FA moiety in all mutant cells. This FA shortening was consistent with our prediction that amino acid residues substituted by SCA34 mutations are located in the transmembrane helices that interact with the ω-end region of the FA moiety of the substrate acyl-CoA. Hence, reduced levels and shortening of ULC-PCs in neurons may cause SCA34, and incomplete elongation of ULC polyunsaturated acyl-CoAs by mutated *ELOVL4* may induce dominant inheritance.

KEYWORDS

33 ELOVL4, spinocerebellar ataxia, fatty acid, neuron, polyunsaturated fatty acid

34

INTRODUCTION

The spinocerebellar ataxias (SCAs) are a group of cerebellar ataxias that are inherited in an autosomal dominant manner and characterized by cerebellar atrophy and ataxia (1, 2). Currently, there exist 49 SCA subtypes; for most of them, causative genes have been identified (1, 3). Each causative gene exhibits a particular type of mutation, such as expansion of CAG repeats encoding the polyglutamine tract, expansion of non-coding repeats, missense mutations, or frameshift mutations (1). It is thought that these mutations have gain-of-function, dominant negative, or loss-of-function (leading to haploinsufficiency) effects. They cause various cellular abnormalities, including transcriptional dysregulation, RNA toxicity, ion channel dysfunction, and mitochondrial dysfunction. One type of SCA, namely SCA34, is caused by mutations in the fatty acid (FA) elongase *ELOVL4*.

ELOVL4 is one of the seven FA elongases (ELOVL1–7) that exist in mammals (4, 5). FAs are classified according to their chain-length; they can be categorized as long-chain FAs (C11–C20) or very-long-chain (VLC) FAs (≥ C21). VLCFAs with C26 or more are termed ultra-long-chain (ULC) FAs (4, 5). FAs are also classified according to their degree of unsaturation and are categorized as saturated FAs (SFAs), monounsaturated FAs (MUFAs), or polyunsaturated FAs (PUFAs). The long-chain FAs synthesized by FA synthase in the cytosol or incorporated from dietary sources are subject to elongation via the FA elongation cycle, which consists of four sequential reactions and takes place in the

endoplasmic reticulum (ER). ELOVLs catalyze the rate-limiting reaction: condensation of an acyl-CoA–the activated form of FA–with a malonyl-CoA (6). Each ELOVL isozyme exhibits characteristic substrate specificity toward acyl-CoAs with different chain-lengths and/or degrees of unsaturation (7). Of the ELOVLs, only ELOVL4 is responsible for generating ULCFAs, regardless of the saturation/unsaturation type (SFAs, MUFAs, and PUFAs) (4, 5, 7). Thus far, five missense mutations—L168F [NM_022726.4(ELOVL4):c.504G>C (p.Leu168Phe), rs587777598], I171T [NM_022726.4(ELOVL4):c.512T>C (p.Ile171Thr), rs1554162301], Q180P [NM_022726.4(ELOVL4):c.539A>C (p.Gln180Pro)], T233M [NM_022726.4(ELOVL4):c.698C>T (p.Thr233Met), rs1554162016], and W246G [NM_022726.4(ELOVL4):c.736T>G (p.Trp246Gly), rs1131692036]—have been identified in *ELOVL4* as mutations that cause SCA34. Gait ataxia, nystagmus, and dysarthria have been reported as common neurological abnormalities in patients with these mutations (8–17). Skin erythrokeratodermia was also observed in patients carrying one of the mutations L168F, Q180P, and T233M (11, 12, 16), while retinitis pigmentosa was observed in a subset of patients harboring the I171T mutation (17). The age of onset differs among the mutations: 10–20 years for Q180P; 10–50 years for T233M and W246G; 30–50 years for I171T; and 30–70 years for L168F. Recently, knock-in (KI) rats harboring the W246G mutation have been generated (18). Assessment using the rotarod performance test revealed that heterozygous and homozygous W246G KI rats exhibited impaired motor function

without apparent histological abnormalities, while homozygous W246G KI rats exhibited impaired synaptic plasticity in parallel and climbing fibers in the cerebellum (18). However, the effects of the SCA34 mutations on ELOVL4 enzymatic activity have not been examined, and the mechanism underlying the pathogenesis and autosomal dominant inheritance mode of SCA34 remains unclear.

Distinct sets of mutations in the *ELOVL4* gene are associated with two other hereditary diseases: Stargardt disease 3 (STGD3) and ISQMR (ichthyosis, spastic quadriplegia, and mental retardation) (19). STGD3 is a type of juvenile macular dystrophy without other neurological or skin symptoms that is inherited in an autosomal dominant manner. Three *ELOVL4* mutations (frameshift mutations N264LfsX10 and N264TfsX9 and the nonsense mutation Y270X) have been identified in STGD3 (20–22). It has been predicted that these mutations produce mutant ELOVL4 proteins lacking the C-terminal of approximately 50 residues, including the ER retention motif. Several studies have demonstrated that these mutant proteins exert dominant negative effects on wild-type (WT) ELVOL4 protein in the retinal photoreceptor cells (23–26). Alternatively, the mutant proteins can be abnormally transported to the outer segment of photoreceptors and phagocytosed by the retinal pigment epithelium, where they cause non-cell-autonomous toxic effects (27, 28). ISQMR is an autosomal recessive neurodevelopmental and cutaneous disorder characterized by skin ichthyosis (scaly and dry skin), spastic quadriplegia, seizures, and intellectual disability. Six *ELOVL4* mutations have been identified in ISQMR (nonsense mutations Y26X, R70X,

and R216X; frameshift mutations I146YfsX29 and I230MfsX22; and the missense mutation C163R) (29–31). R70X and C163R were found together in one compound heterozygous patient, while the other mutations have been found in homozygous patients. Except for C163R, all mutations produce a truncated ELOVL4 protein lacking more C-terminal residues than STGD3 mutant proteins. The C163R mutation causes substitution of the amino acid located near the catalytically essential histidine-motif (residues 158–162). These findings, together with the recessive mode of inheritance, suggest that the ISQMR mutations have loss-of-function effects. Since heterozygous carriers of ISQMR do not exhibit symptoms (29–31), SCA34 is not caused by the simple haploinsufficiency of *ELOVL4*. Other mechanisms may be responsible for rendering the disease dominant.

ELOVL4 is abundantly expressed in the retina, skin, testes, meibomian glands, and brain (mainly in neurons) (32). In the retina, phosphatidylcholines (PCs) containing ULC PUFAs (ULC-PCs) are present and important for visual function (33, 34). In the skin, ULC SFAs/MUFAs are essential for the formation of the epidermal permeability barrier, as they are components of ω-*O*-acylceramides, which are specialized barrier lipids (4, 35, 36). In the testes, ULC PUFAs are used to create glycosphingolipids and sphingomyelins and are essential for spermatogenesis (37). In the meibomian glands, ULC SFAs/MUFAs are used to create cholesteryl esters, wax monoesters/diesters, and (*O*-acyl)-ω-hydroxy FAs, which are secreted as the constituents of tear film lipids and play an important role in preventing dry eye disease (38–42). In the brain, ULC PUFAs are predominantly present in PCs, in

115 which ULC PUFAs with four to six double bonds occupy the *sn*-1 position (43, 44).
116 However, the functions of ULC-PCs in the nervous system and their relationships with
117 SCA34 and ISQMR remain unexplored.

118 The aim of this study was to elucidate the pathogenesis of SCA34 and the molecular
119 mechanism that causes its dominant heritability. For this purpose, we deduced the positions
120 of substituted amino acid residues in ELOVL4 protein based on the recently resolved
121 crystal structure of ELOVL7 (45). We then examined the intracellular localization of
122 mutant proteins and measured the FA elongation activity of the mutant proteins in a
123 cell-based overexpression system. Furthermore, we generated mouse embryonic stem (ES)
124 cells carrying the Q180P or W246G mutation and measured the levels and FA composition
125 of ULC-PCs in them. Through these analyses, we obtained clues about the pathogenesis of
126 SCA34 and the molecular mechanism causing its dominant mode of inheritance.

RESULTS

SCA34 mutations cause amino acid substitutions in the regions involved in the binding of the FA moiety of acyl-CoA in ELOVL4 protein. It has been established that five *ELOVL4* missense mutations cause SCA34 (Fig. 1). However, the position of these amino acid residues in the 3D structure of the ELOVL4 protein remains unclear. In this study, we mapped the amino acid residues of ELOVL4 substituted in SCA34 onto the recently revealed crystal structure of the human ELOVL7 protein (PDB: 6Y7F) (45), which is one of the seven isozymes of the ELOVL family. The amino acid residues of ELOVL4 mutated in SCA34 were L168F, I171T, Q180P, T233M, and W246G, and correspond to residues T157, F160, L169, I222, and F238 from ELOVL7, respectively (Fig. 1). These five residues are not conserved but rather diverged among ELOVL isozymes. In the crystal structure of ELOVL7, these amino acid residues were mapped in the transmembrane helix (TMH) 4 (L168F and I171T), TMH5 (Q180P), TMH6 (T233M), and TMH7 (W246G) (Fig. 2). These residues were not located close to the catalytic site consisting of a histidine box, but rather located at the ω-end region of the FA moiety of the bound acyl-CoA analog (Fig. 2). Thus, the amino acid residues of ELOVL4 substituted in SCA34 constitute the substrate binding site and may participate in the acquisition of substrate specificity in terms of the FA chain length of acyl-CoAs.

SCA34 mutant proteins are localized in the ER. Although WT ELOVL4 is localized in the ER, it has been reported that STGD3 mutations affect its subcellular localization (23, 27). On the other hand, the effect of SCA34 mutations on subcellular localization has not been investigated. To address this, five SCA34 mutants and WT protein as a control were transiently expressed in HeLa cells as 3×FLAG-tagged proteins. Subsequently, their subcellular localization was examined using indirect immunofluorescence microscopy. Consistent with a previous report (7), WT ELOVL4 protein was localized in the ER, as demonstrated by its colocalization with the ER marker calnexin (Fig. 3). All five SCA34 mutant proteins were also localized in the ER, indicating that the SCA34 mutations do not affect intracellular localization.

SCA34 mutants produce shorter ULC lipids than WT ELOVL4. To investigate the effect of SCA34 mutations on the ULCFA-producing activity of ELOVL4, we overproduced 3×FLAG-tagged WT ELOVL4 or each of the SCA34 mutants in HEK 293T cells, extracted the lipids from these cells, and measured the quantities of ceramides and PCs via liquid chromatography (LC)–tandem mass spectrometry (MS/MS). As a control, we also overproduced R216X ISQMR mutant, which lacks a C-terminus (one-third of the protein) and therefore likely has no enzymatic activity. Since ceramides can contain saturated, monounsaturated, or polyunsaturated ULCFA, measurement of ceramides is useful for monitoring the FA elongation activity of ELOVL4 towards each type of

166 acyl-CoA. To produce ULC polyunsaturated ceramides (Fig. 4A), HA-tagged ELOVL2
167 [synthesizes C24 PUFAs (7), the substrates for the synthesis of ULC PUFAs (Fig. 4B)] and
168 3×FLAG-tagged CERS3 [synthesizes ULC ceramides using ULC acyl-CoAs as substrates
169 (46, 47)] were co-overproduced with 3×FLAG-ELOVL4. In the immunoblot analysis, WT
170 ELOVL4 protein was detected as two bands, an upper glycosylated form and a lower
171 non-glycosylated form (Fig. 4C) (7). All five SCA34 mutant proteins were also detected as
172 two bands, with expression levels comparable to that of WT proteins. Two bands of the
173 R216X ISQMR mutant protein were observed (24 and 27 kDa), consistent with the large
174 C-terminus truncation. For the LC–MS/MS analysis, the levels of ceramides produced by
175 each ELOVL4 mutant were shown as a ratio to those produced by WT ELOVL4 and
176 displayed as a heat map (Fig. 4D). In cells expressing the R216X ISQMR mutant, the
177 ceramide composition was similar to that noted in cells transfected with an empty vector.
178 This composition included reduced levels of ≥ C28 saturated/monounsaturated ceramides
179 and ≥ C32 polyunsaturated ceramides, with concomitant increases in the shorter species
180 compared with WT ELOVL4-expressing cells (Fig. 4D and E; E indicates C32:6 and C38:6
181 ceramide levels as representatives). These results demonstrated that as expected, the R216X
182 mutant does not have activity. In cells expressing the SCA34 mutants, the levels of
183 numerous ceramide species containing ≥ C34 ULC PUFA were decreased, accompanied by
184 increases in the levels of ≤ C32 polyunsaturated ceramides (Fig. 4D). An exception to this
185 finding was the L168F mutant; its expression resulted in decreases in most ≥ C30 species,

except C38:4 and C38:5. The chain-length-shortening effect of the SCA mutations was strongest for the Q180P and T233M mutants, followed by W246G, I171T, and L168F. Shortening was also observed for saturated and monounsaturated ceramides by many of the SCA mutants. Nevertheless, shortening was not observed for saturated ceramides by the Q180P mutant and for monounsaturated ceramides by the L168F and I171T mutants.

Next, to measure ULC-PCs (Fig. 4A), which are present in neurons, 3×FLAG-ELOVL4 WT or each of the SCA34 mutants were overexpressed together with HA-ELOVL2 in HEK 293T cells. The expression levels of these proteins were confirmed by immunoblot analysis (Fig. 4F). Lipids were extracted, and ULC-PCs were measured via LC–MS/MS. Each PC species was expressed according to the sum of its chain length and the number of double bonds in its two constituent FAs. Again, PC composition in cells expressing the R216X ISQMR mutant was similar to that recorded in vector-transfected cells (Fig. 4G). Numerous ≥ C50 ULC-PC species were reduced and ≤ C48 species were increased compared with those measured in WT ELOVL4-expressing cells. In the cells expressing the SCA34 mutants, the levels of PCs with ≥ C52 decreased, whereas levels of PCs with ≤ C50 increased in most cases. The heatmap pattern of ULC-PCs for each SCA34 mutant was similar to that of polyunsaturated ceramides (Fig. 4D and G), confirming the above observed activity of SCA34 mutants towards ULC polyunsaturated acyl-CoAs. Comparison of the two heatmaps suggested, for example, that the C32:6 ceramide species corresponds to the C50:7 PC species. Therefore, the C50:7 PC species mainly consists of

206 C32:6 ULC PUFA and C18:1 FA (oleic acid) in the *sn*-1 and *sn*-2 positions, respectively
207 (Fig. 4A). Such PC species have been reported in human and rat brains (43, 44). These
208 results indicate that the SCA34 mutations cause incomplete elongation of ULC
209 polyunsaturated acyl-CoAs and shortening of the ULC PUFA-containing lipids.
210
211 **Neuronal differentiation increases ULC-PC levels.** In the brain, *ELOVL4* is
212 predominantly expressed in neurons (32), and ULC PUFAs synthesized by ELOVL4
213 mainly exist in PCs (43, 44). In the present study, we utilized neurons differentiated from
214 ES cells as model neurons. Mouse ES cells were subjected to differentiation into neurons
215 via the formation of embryoid bodies, treatment with retinoic acids, and growth in neuronal
216 differentiation medium (48). This protocol efficiently induced the differentiation of ES cells
217 into neurons, as demonstrated by their cell morphology and the expression of the neuronal
218 marker class III β-tubulin (Fig. 5A). To confirm *Elovl4* mRNA expression and ULC-PC
219 production in these cells, total RNA and lipids were extracted, and the levels of *Elovl4*
220 mRNAs and ULC-PCs were examined by quantitative RT-PCR and LC–MS/MS,
221 respectively. Both *Elovl4* mRNA and ULC-PC levels increased as the cells differentiated
222 (Fig. 5B and C). Thus, neurons differentiated from ES cells are useful for the evaluation of
223 ELOVL4 activity.
224

225 **Neurons with SCA34 mutations produce shortened ULC-PCs.** To clarify the effects of
226 SCA34 mutations on the levels and composition of ULC-PCs, the Q180P and W246G
227 mutations were each introduced into the *Elovl4* gene in mouse ES cells using
228 single-stranded oligodeoxynucleotide-mediated KI with a CRISPR/Cas9 system (49).
229 These mutations were selected as severe (Q180P) and moderate (W246G) examples in
230 terms of the age of disease onset (12, 50) and their shortening effect on ULC-lipids (Fig. 4).
231 A heterozygous KI clone, which mimics the dominant form of inheritance in SCA34, was
232 obtained for each mutation. A homozygous KI clone, which likely exhibits more changes
233 than the corresponding heterozygous KI clone, was obtained for the W246G mutation (Fig.
234 6A). These KI and control ES cells were differentiated into neurons, and the lipids prepared
235 after 1 and 5 days of differentiation were subjected to quantification of ULC-PCs by LC–
236 MS/MS. After 1 day of differentiation, the total levels of ULC-PCs in W246G homozygous
237 KI cells were reduced to 42% of those noted in control cells (Fig. 6B). On the other hand,
238 heterozygous Q180P and W246G cells exhibited reduction tendencies, which were not
239 statistically significant. The proportion of ≥ C52 ULC-PCs, which mainly consists of ≥ C34
240 ULC PUFAs, among the total ULC-PCs was lower in Q180P heterozygous and W246G
241 homozygous KI cells than in control cells. These findings were suggestive of ULC PUFA
242 shortening. The proportion of ≥ C52 ULC-PCs in W246G heterozygous KI cells was
243 slightly higher than that recorded in control cells at this early stage of differentiation. After
244 5 days of differentiation, total ULC-PC levels had reduced significantly in W246G

245 homozygous KI cells (reduction to 43%) and Q180P heterozygous KI cells (reduction to
246 44%). On the other hand, W246G heterozygous KI cells exhibited a reduction tendency,
247 which was not statistically significant. The proportions of ≥ C52 ULC-PCs in all three KI
248 cells were lower than that measured in control cells. The observed reduction and shortening
249 of ULC-PCs in KI cells were not due to the reduced expression of *Elovl* genes involved in
250 the synthesis of ULC PUFA or defective differentiation into neurons. This conclusion is
251 based on a lack of reduced expression levels of *Elovl4*, *Elovl2*, *Elovl5*, and the neuronal
252 differentiation marker *Tubb3* (encodes class III β-tubulin) in the KI cells after 5 days of
253 differentiation (Fig. 6C). Rather, increases in the levels of *Elovl4* and *Tubb3* in Q180P
254 heterozygous KI cells and in those of *Elovl2* in W246G heterozygous KI cells were
255 observed. These results indicate that polyunsaturated acyl-CoA elongation is incomplete in
256 neurons possessing SCA34 mutations and suggest that decreases and/or shortening of
257 ULC-PCs are associated with the pathogenesis of SCA34.
258

DISCUSSION

Five *ELOVL4* missense mutations have been identified in patients with SCA34 (12, 15, 50). In the present study, all five amino acid residues substituted in SCA34 were mapped to TMHs that interact with the ω-end region of the FA moiety of the substrate acyl-CoA based on the 3D structure of ELOVL7 (Fig. 2) (45). WT ELOVL4 protein exhibits activity for the elongation of C24 or C26 acyl-CoA to become C36 or C38 (Fig. 4) (4, 51). This indicates that its substrate-binding pocket has sufficient space to accommodate a C36 or C38 ULC acyl-CoA. Each of the SCA34 mutations may alter the pocket structure so that it can only accommodate shorter ULC acyl-CoAs, leading to incomplete elongation of acyl-CoAs (in the case of polyunsaturated acyl-CoAs, up to C32; Figs 4 and 6). The effects of the Q180P, T233M, and W246G mutations on the elongation of polyunsaturated ULC acyl-CoA were greater than those of L168F and I171T (Fig. 4). There was thus a correlation between the degree of ULC-PC shortening and the age of disease onset (see Introduction) (12, 50). The Q180P mutation affected the elongation of polyunsaturated and monounsaturated ULC acyl-CoAs, but did not affect saturated ULC acyl-CoAs (Fig. 4). The Gln180 residue is present in TMH5, so its α-helix structure is likely disrupted by the Gln-to-Pro substitution, leading to a structural change in the substrate-binding pocket that alters the substrate specificity depending on the saturation/unsaturation status.

In this study, we found that the levels of ≥ C52 PCs were lower in Q180P and W246G heterozygous KI neurons compared with control neurons (Fig. 6B). In addition, Q180P

279 heterozygous KI neurons showed a decrease in total ULC-PC levels. These results suggest
280 that the shortening of ULC PUFAs and reduction in ULC-PCs in neurons are involved in
281 the pathogenesis of SCA34. The shortening of ULC PUFAs is particularly important, since
282 it was observed in all five SCA34 mutations (Fig. 4). The ≥ C52 ULC-PCs may play an
283 important role in neuronal functions; hence, they cannot be replaced by shorter ULC-PCs.
284 Although the presence of ULC-PCs has long been recognized (33, 34), their function in
285 neurons remains unknown. Neurons like the Purkinje cells in the cerebellum have very
286 complex structures, including highly branched neurites and synapses. Given the special
287 structure of ULC-PCs, with a ULC PUFA in the *sn*-1 position, they may be enriched in
288 membranes that make up complex structures like neurites and synapses, and the shortening
289 of ULC PUFAs may impair their function in these structures.

290 In this study, we also analyzed the R216X mutation, one of the causative mutations in
291 recessively inherited ISQMR. In a cell-based assay, the R216X mutant did not exhibit
292 activity for the production of ULC ceramides or ULC-PCs (Fig. 4). Thus, the R216X
293 mutation has a loss-of-function effect, which is consistent with the recessive inheritance
294 mode of ISQMR. Since the R216X mutant lacks TMH6 and subsequently the C-terminal
295 region, it cannot form the substrate-binding pocket for acyl-CoAs.

296 Although the R216X ISQMR mutant did not exhibit activity, SCA34 mutants had
297 residual activity. The neurological symptoms of ISQMR are severe and become evident
298 within the first few months to 1 year after birth (29). In contrast, the symptoms of SCA34

299 are milder than those of ISQMR, with the onset of disease mostly observed in middle age
300 (12, 50). Thus, SCA34 pathology may develop due to long-term decreases and/or changes
301 in the quality (shortening) of ULC-PCs in neurons in the cerebellum, which may be more
302 susceptible than other brain regions.

303 We speculate that the cause of the dominant inheritance mode of SCA34 is the
304 substitution of highly functional ≥ C52 ULC-PCs (ULCFA moiety, mainly ≥ C34) for
305 weakly functional ≤ C50 ULC-PCs (ULCFA moiety, mainly ≤C32) (Fig. 7). This
306 substitution may be related to the continuity of acyl-CoA elongation in the FA elongation
307 cycle involving ELOVL4. The FA elongation cycle consists of four sequential reactions
308 starting from condensation by ELOVLs, then reduction by 3-ketoacyl-CoA reductase,
309 dehydration by 3-hydroxyacyl-CoA reductases, and reduction by *trans*-2-enoyl-CoA
310 reductase (4, 5). These are all ER-resident proteins and may form complexes (4, 25, 52),
311 which enables efficient and sequential progress of reactions. Since ELOVL4 is the only
312 enzyme involved in the elongation of ULC acyl-CoAs from C24 or C26 to C34–C38, it is
313 reasonable to assume that the acyl-CoA synthesized in the previous cycle enters the next
314 cycle catalyzed by the same complex, rather than dissociate from the previous complex and
315 find and associate with another complex. Thus, one C24/C26 acyl-CoA may be elongated
316 repetitively to become C34–C38 by the same ELOVL4-containing complex (Fig. 7).
317 However, it is likely that C24/C26 acyl-CoA may be elongated only up to C32 by
318 FA-elongation complexes that contain an SCA34 mutant; they would then be released from

319 the complex and used for PC synthesis. Although carriers that are heterozygous for the
320 ISQMR mutation are predicted to have half the ELOVL4 activity of normal individuals,
321 they do not develop symptoms (29–31). This may be because ULC acyl-CoAs are fully
322 elongated by the remaining WT ELOVL4 (Fig. 7). In other words, SCA34 is induced by
323 shortening of ULC PUFAs due to incomplete elongation reactions, rather than decreased
324 activity of ELOVL4.

325 In summary, this is the first biochemical analysis of SCA34 mutations, and our
326 findings suggest that the molecular mechanism underlying the pathogenesis of SCA34 is a
327 decrease in the levels and/or shortening of ULC-PCs. Furthermore, the dominant
328 inheritance mode of SCA34 is caused by the substitution of ≥ C52 ULC-PCs with ≤ C50
329 ULC-PCs. Another SCA subtype, namely SCA38, is caused by mutations in *ELOVL5* (53–
330 55), which is responsible for the elongation of polyunsaturated acyl-CoAs from C18 to C22
331 (Fig. 4B) (4, 5, 7). This suggests a link between SCA34 and SCA38 and raises the
332 possibility that the neural symptoms in these disorders are caused by the same or a similar
333 molecular mechanism (that is to say, the shortening of ULC-PCs). Future research is
334 needed to investigate whether SCA38 and other SCA subtypes are also accompanied by
335 changes in the quantity or quality of ULC-PCs.

MATERIALS AND METHODS

Amino acid mapping. Five amino acid residues of ELOVL4 that are substituted in SCA34 were mapped onto the crystal structure of human ELOVL7 (PDB ID: 6Y7F) using PyMOL software (version 2.5.2; Schrödinger, New York, NY, USA).

Plasmids. The mammalian expression vectors pEFh-3×FLAG-1 (56) and pCE-puro 3×FLAG-1 (57) were used for the expression of N-terminally 3×FLAG-tagged proteins, while the mammalian expression vector pCE-puro HA-1 (52) was used for the expression of N-terminally HA-tagged protein. The pCE-puro 3×FLAG-CERS3 and pCE-puro HA-ELOVL2 plasmids have been described previously (52, 58). The pEFh-3×FLAG-ELOVL4 plasmid was constructed by transferring *ELOVL4* from pCE-puro 3×FLAG-ELOVL4 (59) to the pEFh-3×FLAG-1 vector. The *ELOVL4* mutants were generated via overlap extension PCR using pCE-puro 3×FLAG-ELOVL4 plasmid as a template and primers (Table 1), followed by cloning into the pEFh-3×FLAG-1 vector to produce pEFh-3×FLAG-mutated ELOVL4 plasmids.

The all-in-one CRISPR/Cas9 vector pYU751 consists of a WT *Cas9* nuclease, a guide RNA (gRNA) cloning cassette, *EGFP*, and the gene that encodes puromycin *N*-acetyltransferase. This vector was constructed from the GeneArt CRISPR Nuclease Vector with the OFP plasmid (Thermo Fisher Scientific, Waltham, MA, USA) by incorporating the puromycin *N*-acetyltransferase gene and substituting the *ORF* reporter

with *EGFP*. To generate Q180P and W246G *Elovl4* KI mouse ES cells, a pair of oligonucleotides (Table 2) encoding gRNAs targeting exon 4 (for Q180P) and exon 6 (for W246G) of *Elovl4* were annealed and cloned into the *Bae*I site of pYU751, generating the plasmids pUKA27 and pUKA16, respectively.

Cell culture and transfection. HEK 293T cells (RCB2202; Riken BioResouce Research Center, Tsukuba, Japan) and HeLa cells (RCB0007; Riken BioResouce Research Center) were cultured in Dulbecco's Modified Eagle's Medium containing 4,500 mg/L glucose (D6429; Merck, Darmstadt, Germany) and 1,000 mg/L glucose (D6046; Merck), respectively, supplemented with 10% FBS, 100 units/mL penicillin, and 100 μg/mL streptomycin. HEK 293T cells were grown on collagen-coated dishes. E14tg2a mouse ES cells (AES0135; Riken BioResouce Research Center) were cultured in Glasgow's MEM (Thermo Fisher Scientific) that was supplemented with 10% FBS, 0.1 mM MEM Non-Essential Amino Acids Solution (Thermo Fisher Scientific), 1 mM sodium pyruvate (Thermo Fisher Scientific), 0.1 mM 2-mercaptoethanol (FUJIFILM Wako Pure Chemical, Osaka, Japan), 1,000 units/mL mouse Leukemia Inhibitory Factor (FUJIFILM Wako Pure Chemical), 100 units/mL penicillin, and 100 μg/mL streptomycin, and were grown on a 0.1% gelatin-coated dish. All cells were cultured at 37 °C in 5% CO_2 and used in less than 20 passages. Transfections were performed using Lipofectamine Transfection Reagent with PLUS Reagent (Thermo Fisher Scientific) according to the manufacturer's instructions.

Indirect immunofluorescence microscopy. HeLa cells and differentiated ES cells were subjected to indirect immunofluorescence microscopy as previously described (60). Rabbit anti-FLAG polyclonal antibody (1:2,000 dilution) (61), mouse anti-calnexin monoclonal PM060 antibody (RRID: AB_10597560; 1:400 dilution; Medical & Biological Laboratories, Tokyo, Japan), and mouse anti-class III β-tubulin monoclonal MAB1195 antibody (RRID: AB_357520; 1:500 dilution; R&D Systems, Minneapolis, USA) were used as primary antibodies. Alexa Fluor 488-conjugated anti-mouse IgG antibody (RRID: AB_2534069) and Alexa Fluor 594-conjugated anti-rabbit IgG antibody (RRID: AB_2534073; each 1:200 dilution; Thermo Fisher Scientific) were used as secondary antibodies, and DAPI (1 μg/mL) was added simultaneously. Cover slips were mounted with ProLong Gold Antifade Reagent (Thermo Fisher Scientific) and observed using a Leica DM5000B microscope (Leica Microsystems, Wetzlar, Germany).

Immunoblotting. Immunoblotting was performed as previously described (60), using rabbit anti-FLAG polyclonal antibody (1:1,000 dilution) (61) and mouse anti-α-tubulin monoclonal T9026 antibody (RRID: AB_477593; 1:1,000 dilution; Merck) as primary antibodies and anti-rabbit and anti-mouse IgG, HRP-linked $F(ab')_2$ fragments (each 1:7,500 dilution; GE Healthcare Life Sciences, Little Chalfont, UK) as secondary antibodies. Chemiluminescence detection was performed using chemiluminescence solution; this

396 solution consisted of 100 mM Tris-HCl (pH 8.5), 0.2 mM *p*-coumaric acid (Merck), 2.5
397 mM luminol (FUJIFILM Wako Pure Chemical), and 0.002% hydrogen peroxide.
398
399 **Generation of SCA34 KI ES cells.** For homology-directed repair, the single-stranded
400 oligodeoxynucleotides (ssODNs) mElovl4Q180P_ssODN and mElovl4W246G_ssODN
401 were designed. Each ssODN contained the mutant sequence and bilateral homology arms
402 for homology-directed repair in ES cells (Table 3). For each ssODN, the non-target strand,
403 which was not complementary to the gRNA, was chosen to avoid heteroduplex formation
404 with gRNA (49). In the mutant sequence, mElovl4Q180P_ssODN and
405 mElovl4W246G_ssODN contained *Apa*I and *Sph*I restriction enzyme sites, respectively;
406 these were introduced to examine the presence of mutations at the *Elovl4* locus. To obtain
407 *Elovl4* Q180P KI cells and W246G KI cells, ES cells were transfected with pUKA27 and
408 mElovl4Q180P_ssODN (for Q180P KI cells), pUKA16 and mElovl4_W246G_ssODN (for
409 W246G KI cells), or empty pYU751 vectors (as controls). Twenty-four hours after
410 transfection, the cells were treated with 2 μg/mL puromycin and incubated for another 24 h
411 to eliminate untransfected cells. The cells that survived were subsequently diluted and
412 cultured in the absence of puromycin for 9 days. Single colonies were isolated using
413 cloning rings, then expanded and stored. Genomic DNAs were extracted from the cells, and
414 the DNA fragments containing the target sites were amplified by PCR. The amplified DNA
415 fragments were digested with restriction enzymes (*Apa*I for Q180P and *Sph*I for W246G) to

examine the presence of the mutations. Positive clones identified by restriction enzyme analysis were subjected to sequence confirmation by Sanger sequencing.

Neuronal differentiation of ES cells. Embryoid bodies were formed by growing ES cells in embryoid body formation medium; this mixture consisted of equal volumes of Advanced DMEM/F12 (Thermo Fisher Scientific) and Neurobasal Medium (Thermo Fisher Scientific), supplemented with 10% KnockOut Serum Replacement (Thermo Fisher Scientific), 2 mM L-glutamine (Thermo Fisher Scientific), 100 units/mL penicillin, 100 μg/mL streptomycin, and 0.1 mM 2-mercaptoethanol. Two days later, the embryoid bodies were cultured in embryoid body formation medium that was supplemented with 5 μM retinoic acid. Three days later, differentiation of the embryoid bodies into neurons was induced by replacing the medium with neuronal differentiation medium. This medium consisted of a mixture of equal volumes of Advanced DMEM/F12 and Neurobasal Medium, supplemented with 2% B-27 Supplement (Thermo Fisher Scientific), 2 mM L-glutamine, 100 units/mL penicillin, and 100 μg/mL streptomycin. On the following day, the embryoid bodies were digested with 0.25% Trypsin/EDTA (Merck), dispersed in Leibovitz's L-15 Medium (Thermo Fisher Scientific) supplemented with 0.2 mg/mL DNase I (Merck), and seeded onto a poly-D-lysine/laminin-coated dish in the neuronal differentiation medium for an additional 4 days.

436 **Lipid analyses.** For the analysis of ceramides and PCs, HEK 293T cells were transfected
437 with the following combinations of plasmids: pEFh-3×FLAG-ELOVL4 (WT or one of the
438 mutants), pCE-puro 3×FLAG-CERS3, and pCE-puro HA-ELOVL2 plasmids for analysis
439 of ceramides; pEFh-3×FLAG-ELOVL4 (WT or one of the mutants) and pCE-puro
440 HA-ELOVL2 plasmids for analysis of PCs. Forty-eight hours after transfection, cells were
441 collected and subjected to lipid extraction.

442 For the extraction of ceramides from HEK 293T cells, the cells were suspended in 100
443 μL of water and mixed successively with 375 μL of chloroform/methanol/12 M formic acid
444 solution (100:200:1, v/v), 125 μL of chloroform, and 125 μL of water. After centrifugation,
445 the organic phase was recovered and treated with 71 μL of 0.5 M NaOH for 1 h at 37 °C to
446 hydrolyze ester bonds in the glycerolipids. The reaction mixture was neutralized via the
447 addition of 35.5 μL of 1 M formic acid and mixed successively with 135 μL of methanol
448 and 210 μL of water. After centrifugation, the organic phase was recovered and dried. For
449 the extraction of PCs from HEK 293T or ES cells, the cells were suspended in 100 μL of
450 water and mixed successively with 375 μL of chloroform/methanol/12 M formic acid
451 solution (100:200:1, v/v), 0.5 pmol of seven deuterium (d_7)-labeled internal standard
452 (15:0/18:1-d_7-PC; Avanti Polar Lipids, Alabaster, USA), 125 μL of chloroform, and 125 μL
453 of water. After centrifugation, the organic phase was recovered and dried.

454 The dried lipids were suspended in a chloroform/methanol solution (1:2, v/v), and LC–
455 MS/MS analyses of ceramides and PCs were performed using an LC-coupled triple

quadrupole mass spectrometer Xevo TQ-S (Waters, Milford, MA, USA). Ceramides and PCs extracted from HEK 293T cells were separated by LC using an ACQUITY UPLC CSH C18 column (1.7 μm particle size, 2.1 × 100 mm; Waters), and PCs extracted from ES cells were separated by LC using a YMC-Triant C18 metal-free column (1.9 μm particle size, 2.1 × 50 mm; YMC, Kyoto, Japan). Lipid separation by LC was performed at a flow rate of 0.3 mL/min for 25 min using a gradient system, in which mobile phase A and mobile phase B were mixed as follows: 0 min, 40% B; 0–18 min, gradient to 100% B; 18–23 min, 100% B; 23 min, return to 40% B; 23–25 min, 40% B. Mobile phase A consisted of an acetonitrile/water solution (3:2, v/v) that contained 5 mM ammonium formate, while mobile phase B consisted of an acetonitrile/2-propanol solution (1:9, v/v) that contained 5 mM ammonium formate. Separated lipids were ionized by electrospray ionization and analyzed in positive ion mode. Quantitative analyses were performed in the multiple reaction monitoring mode of the MS/MS using selected *m/z* values and appropriate collision energies and cone voltages (Tables 4 and 5). Data analyses were performed using MassLynx software (Waters). Ceramides were quantified using the external standard curve generated from C30:0 ceramide (Cayman Chemical, Ann Arbor, MI, USA) and expressed as the proportion of each ceramide species to the sum of all measured ceramide species listed in Table 4. PCs were quantified by calculating the ratio of the peak area of each PC species to that of the internal standard (15:0/18:1-d_7-PC).

476 **Real-time quantitative RT-PCR.** Total RNAs were isolated from ES cells using the
477 NucleoSpin RNA Kit (Takara Bio, Kusatsu, Japan), and cDNAs were synthesized from
478 total RNAs using the PrimeScript II 1st strand cDNA Synthesis Kit (Takara Bio). Real-time
479 quantitative RT-PCR was performed using the KOD SYBR qPCR Mix (TOYOBO, Osaka,
480 Japan), cDNAs, and specific forward and reverse primers for the respective genes (Table 6).
481 The reaction was performed on a CFX96 Touch real-time PCR detection system (Bio-Rad,
482 Hercules, CA, USA). The mRNA levels were normalized to that of *Actb*.
483
484 **Quantification and statistical analysis.** Data are presented as means + SD. Tests for
485 normality of the data and outliers were not performed. Differences between groups were
486 evaluated using Dunnett's test in JMP 13 software (SAS Institute, Cary, NC, USA), and
487 *p*-values of less than 0.05 were considered to be statistically significant.
488
489 **Ethical approval.** No ethical approval was required for this study.
490

ACKNOWLEDGEMENTS

This work was supported by KAKENHI grants: grant numbers JP22H04986 (to A.K.) and JP22H02757 (to T.S.) from the Japan Society for the Promotion of Science (JSPS) and by a Grant for Basic Science Research Projects (to T.S.) from the Sumitomo Foundation.

REFERENCES

1. Robinson KJ, Watchon M, Laird AS. 2020. Aberrant cerebellar circuitry in the spinocerebellar ataxias. Front Neurosci 14:707. https://doi.org/10.3389/fnins.2020.00707

2. Sullivan R, Yau WY, O'Connor E, Houlden H. 2019. Spinocerebellar ataxia: an update. J Neurol 266:533–544. https://doi.org/10.1007/s00415-018-9076-4

3. Corral-Juan M, Casquero P, Giraldo-Restrepo N, Laurie S, Martinez-Piñeiro A, Mateo-Montero RC, Ispierto L, Vilas D, Tolosa E, Volpini V, Alvarez-Ramo R, Sánchez I, Matilla-Dueñas A. 2022. New spinocerebellar ataxia subtype caused by *SAMD9L* mutation triggering mitochondrial dysregulation (SCA49). Brain Commun 4:fcac030. https://doi.org/10.1093/braincomms/fcac030

4. Kihara A. 2016. Synthesis and degradation pathways, functions, and pathology of ceramides and epidermal acylceramides. Prog Lipid Res 63:50–69. https://doi.org/10.1016/j.plipres.2016.04.001

5. Sassa T, Kihara A. 2014. Metabolism of very long-chain fatty acids: genes and pathophysiology. Biomol Ther 22:83–92. https://doi.org/10.4062/biomolther.2014.017

6. Bernert JT, Jr., Sprecher H. 1977. An analysis of partial reactions in the overall chain elongation of saturated and unsaturated fatty acids by rat liver microsomes. J Biol Chem 252:6736–6744. https://doi.org/10.1016/S0021-9258(17)39911-8

7. Ohno Y, Suto S, Yamanaka M, Mizutani Y, Mitsutake S, Igarashi Y, Sassa T, Kihara A. 2010. ELOVL1 production of C24 acyl-CoAs is linked to C24 sphingolipid synthesis. Proc Natl Acad Sci U S A 107:18439–18444. https://doi.org/10.1073/pnas.1005572107

8. Beaudin M, Sellami L, Martel C, Touzel-Deschênes L, Houle G, Martineau L, Lacroix K, Lavallée A, Chrestian N, Rouleau GA, Gros-Louis F, Laforce R, Jr., Dupré N. 2020. Characterization of the phenotype with cognitive impairment and protein mislocalization in SCA34. Neurol Genet 6:e403. https://doi.org/10.1212/NXG.0000000000000403

9. Bourassa CV, Raskin S, Serafini S, Teive HA, Dion PA, Rouleau GA. 2015. A new *ELOVL4* mutation in a case of spinocerebellar ataxia with erythrokeratodermia. JAMA Neurol 72:942–943. https://doi.org/10.1001/jamaneurol.2015.0888

10. Bourque PR, Warman-Chardon J, Lelli DA, LaBerge L, Kirshen C, Bradshaw SH, Hartley T, Boycott KM. 2018. Novel *ELOVL4* mutation associated with erythrokeratodermia and spinocerebellar ataxia (SCA 34). Neurol Genet 4:e263. https://doi.org/10.1212/NXG.0000000000000263

11. Cadieux-Dion M, Turcotte-Gauthier M, Noreau A, Martin C, Meloche C, Gravel M, Drouin CA, Rouleau GA, Nguyen DK, Cossette P. 2014. Expanding the clinical phenotype associated with *ELOVL4* mutation: study of a large French-Canadian

family with autosomal dominant spinocerebellar ataxia and erythrokeratodermia. JAMA Neurol 71:470–475. https://doi.org/10.1001/jamaneurol.2013.6337

12. Haeri G, Hajiakhoundi F, Alavi A, Ghiasi M, Munhoz RP, Rohani M. 2021. Congenital ichthyosis in a case of spinocerebellar ataxia type 34: a novel presentation for a known mutation. Mov Disord Clin Pract 8:275–278. https://doi.org/10.1002/mdc3.13123

13. Mukherjee S, Roy M, Ghosh S, Guha G, Prasad Saha S, Dalal A. 2021. Rare mutation in ELOVL4 gene in SCA34 and cognitive affection: Expounding the role of cerebellum. Clin Neurol Neurosurg 210:106983. https://doi.org/10.1016/j.clineuro.2021.106983

14. Ozaki K, Ansai A, Nobuhara K, Araki T, Kubodera T, Ishii T, Higashi M, Sato N, Soga K, Mizusawa H, Ishikawa K, Yokota T. 2019. Prevalence and clinicoradiological features of spinocerebellar ataxia type 34 in a Japanese ataxia cohort. Parkinsonism Relat Disord 65:238–242. https://doi.org/10.1016/j.parkreldis.2019.05.019

15. Ozaki K, Doi H, Mitsui J, Sato N, Iikuni Y, Majima T, Yamane K, Irioka T, Ishiura H, Doi K, Morishita S, Higashi M, Sekiguchi T, Koyama K, Ueda N, Miura Y, Miyatake S, Matsumoto N, Yokota T, Tanaka F, Tsuji S, Mizusawa H, Ishikawa K. 2015. A novel mutation in *ELOVL4* leading to spinocerebellar ataxia (SCA) with the

554 hot cross bun sign but lacking erythrokeratodermia: a broadened spectrum of SCA34.
555 JAMA Neurol 72:797–805. https://doi.org/10.1001/jamaneurol.2015.0610
556 16. Wang Z, Lin Z, Wang H. 2021. Progressive symmetric erythrokeratodermia with
557 spinocerebellar ataxia due to *ELOVL4* mutation in a Chinese family. Indian J
558 Dermatol Venereol Leprol 88:132. https://doi.org/10.25259/ijdvl_488_20
559 17. Xiao C, Binkley EM, Rexach J, Knight-Johnson A, Khemani P, Fogel BL, Das S,
560 Stone EM, Gomez CM. 2019. A family with spinocerebellar ataxia and retinitis
561 pigmentosa attributed to an *ELOVL4* mutation. Neurol Genet 5:e357.
562 https://doi.org/10.1212/nxg.0000000000000357
563 18. Nagaraja RY, Sherry DM, Fessler JL, Stiles MA, Li F, Multani K, Orock A, Ahmad
564 M, Brush RS, Anderson RE, Agbaga MP, Deák F. 2021. W246G mutant ELOVL4
565 impairs synaptic plasticity in parallel and climbing fibers and causes motor defects in
566 a rat model of SCA34. Mol Neurobiol 58:4921–4943.
567 https://doi.org/10.1007/s12035-021-02439-1
568 19. Hopiavuori BR, Anderson RE, Agbaga MP. 2019. ELOVL4: Very long-chain fatty
569 acids serve an eclectic role in mammalian health and function. Prog Retin Eye Res
570 69:137–158. https://doi.org/10.1016/j.preteyeres.2018.10.004
571 20. Bernstein PS, Tammur J, Singh N, Hutchinson A, Dixon M, Pappas CM, Zabriskie
572 NA, Zhang K, Petrukhin K, Leppert M, Allikmets R. 2001. Diverse macular

573 dystrophy phenotype caused by a novel complex mutation in the *ELOVL4* gene.
574 Invest Ophthalmol Vis Sci 42:3331–3336.
575 21. Maugeri A, Meire F, Hoyng CB, Vink C, Van Regemorter N, Karan G, Yang Z,
576 Cremers FP, Zhang K. 2004. A novel mutation in the *ELOVL4* gene causes autosomal
577 dominant Stargardt-like macular dystrophy. Invest Ophthalmol Vis Sci 45:4263–4267.
578 https://doi.org/10.1167/iovs.04-0078
579 22. Zhang K, Kniazeva M, Han M, Li W, Yu Z, Yang Z, Li Y, Metzker ML, Allikmets R,
580 Zack DJ, Kakuk LE, Lagali PS, Wong PW, MacDonald IM, Sieving PA, Figueroa DJ,
581 Austin CP, Gould RJ, Ayyagari R, Petrukhin K. 2001. A 5-bp deletion in *ELOVL4* is
582 associated with two related forms of autosomal dominant macular dystrophy. Nat
583 Genet 27:89–93. https://doi.org/10.1038/83817
584 23. Grayson C, Molday RS. 2005. Dominant negative mechanism underlies autosomal
585 dominant Stargardt-like macular dystrophy linked to mutations in ELOVL4. J Biol
586 Chem 280:32521–32530. https://doi.org/10.1074/jbc.m503411200
587 24. Karan G, Yang Z, Howes K, Zhao Y, Chen Y, Cameron DJ, Lin Y, Pearson E, Zhang
588 K. 2005. Loss of ER retention and sequestration of the wild-type ELOVL4 by
589 Stargardt disease dominant negative mutants. Mol Vis 11:657–664.
590 25. Okuda A, Naganuma T, Ohno Y, Abe K, Yamagata M, Igarashi Y, Kihara A. 2010.
591 Hetero-oligomeric interactions of an ELOVL4 mutant protein: implications in the
592 molecular mechanism of Stargardt-3 macular dystrophy. Mol Vis 16:2438–2445.

593 26. Vasireddy V, Vijayasarathy C, Huang J, Wang XF, Jablonski MM, Petty HR, Sieving
594 PA, Ayyagari R. 2005. Stargardt-like macular dystrophy protein ELOVL4 exerts a
595 dominant negative effect by recruiting wild-type protein into aggresomes. Mol Vis
596 11:665–676.
597 27. Esteve-Rudd J, Hazim RA, Diemer T, Paniagua AE, Volland S, Umapathy A,
598 Williams DS. 2018. Defective phagosome motility and degradation in cell
599 nonautonomous RPE pathogenesis of a dominant macular degeneration. Proc Natl
600 Acad Sci U S A 115:5468–5473. https://doi.org/10.1073/pnas.1709211115
601 28. Kuny S, Cho WJ, Dimopoulos IS, Sauvé Y. 2015. Early onset ultrastructural and
602 functional defects in RPE and photoreceptors of a Stargardt-like macular dystrophy
603 (STGD3) transgenic mouse model. Invest Ophthalmol Vis Sci 56:7109–7121.
604 https://doi.org/10.1167/iovs.15-17567
605 29. Aldahmesh MA, Mohamed JY, Alkuraya HS, Verma IC, Puri RD, Alaiya AA, Rizzo
606 WB, Alkuraya FS. 2011. Recessive mutations in *ELOVL4* cause ichthyosis,
607 intellectual disability, and spastic quadriplegia. Am J Hum Genet 89:745–750.
608 https://doi.org/10.1016/j.ajhg.2011.10.011
609 30. Diociaiuti A, Martinelli D, Nicita F, Cesario C, Pisaneschi E, Macchiaiolo M, Rossi S,
610 Condorelli AG, Zambruno G, El Hachem M. 2021. Two Italian patients with
611 *ELOVL4*-related neuro-ichthyosis: expanding the genotypic and phenotypic spectrum

612 and ultrastructural characterization. Genes 12:343.
613 https://doi.org/10.3390/genes12030343
614 31. Mir H, Raza SI, Touseef M, Memon MM, Khan MN, Jaffar S, Ahmad W. 2014. A
615 novel recessive mutation in the gene ELOVL4 causes a neuro-ichthyotic disorder
616 with variable expressivity. BMC Med Genet 15:25.
617 https://doi.org/10.1186/1471-2350-15-25
618 32. Sherry DM, Hopiavuori BR, Stiles MA, Rahman NS, Ozan KG, Deak F, Agbaga MP,
619 Anderson RE. 2017. Distribution of ELOVL4 in the developing and adult mouse
620 brain. Front Neuroanat 11:38. https://doi.org/10.3389/fnana.2017.00038
621 33. Bennett LD, Brush RS, Chan M, Lydic TA, Reese K, Reid GE, Busik JV, Elliott MH,
622 Anderson RE. 2014. Effect of reduced retinal VLC-PUFA on rod and cone
623 photoreceptors. Invest Ophthalmol Vis Sci 55:3150–3157.
624 https://doi.org/10.1167/iovs.14-13995
625 34. Harkewicz R, Du H, Tong Z, Alkuraya H, Bedell M, Sun W, Wang X, Hsu YH,
626 Esteve-Rudd J, Hughes G, Su Z, Zhang M, Lopes VS, Molday RS, Williams DS,
627 Dennis EA, Zhang K. 2012. Essential role of ELOVL4 protein in very long chain
628 fatty acid synthesis and retinal function. J Biol Chem 287:11469–11480.
629 https://doi.org/10.1074/jbc.m111.256073
630 35. Li W, Sandhoff R, Kono M, Zerfas P, Hoffmann V, Ding BC, Proia RL, Deng CX.
631 2007. Depletion of ceramides with very long chain fatty acids causes defective skin

632 permeability barrier function, and neonatal lethality in ELOVL4 deficient mice. Int J
633 Biol Sci 3:120–128. https://doi.org/10.7150/ijbs.3.120
634 36. Vasireddy V, Uchida Y, Salem N, Jr., Kim SY, Mandal MN, Reddy GB, Bodepudi R,
635 Alderson NL, Brown JC, Hama H, Dlugosz A, Elias PM, Holleran WM, Ayyagari R.
636 2007. Loss of functional ELOVL4 depletes very long-chain fatty acids (≥C28) and
637 the unique ω-O-acylceramides in skin leading to neonatal death. Hum Mol Genet
638 16:471–482. https://doi.org/10.1093/hmg/ddl480
639 37. Rabionet M, Bayerle A, Jennemann R, Heid H, Fuchser J, Marsching C, Porubsky S,
640 Bolenz C, Guillou F, Gröne HJ, Gorgas K, Sandhoff R. 2015. Male meiotic
641 cytokinesis requires ceramide synthase 3-dependent sphingolipids with unique
642 membrane anchors. Hum Mol Genet 24:4792–4808.
643 https://doi.org/10.1093/hmg/ddv204
644 38. McMahon A, Lu H, Butovich IA. 2014. A role for ELOVL4 in the mouse meibomian
645 gland and sebocyte cell biology. Invest Ophthalmol Vis Sci 55:2832–2840.
646 https://doi.org/10.1167/iovs.13-13335
647 39. Miyamoto M, Sassa T, Sawai M, Kihara A. 2020. Lipid polarity gradient formed by
648 ω-hydroxy lipids in tear film prevents dry eye disease. eLife 9:e53582.
649 https://doi.org/10.7554/elife.53582

650 40. Otsuka K, Sawai-Ogawa M, Kihara A. 2022. Formation of fatty alcohols-components
651 of meibum lipids-by the fatty acyl-CoA reductase FAR2 is essential for dry eye
652 prevention. FASEB J 36:e22216. https://doi.org/10.1096/fj.202101733r
653 41. Sassa T, Tadaki M, Kiyonari H, Kihara A. 2018. Very long-chain tear film lipids
654 produced by fatty acid elongase ELOVL1 prevent dry eye disease in mice. FASEB J
655 32:2966–2978. https://doi.org/10.1096/fj.201700947r
656 42. Sawai M, Watanabe K, Tanaka K, Kinoshita W, Otsuka K, Miyamoto M, Sassa T,
657 Kihara A. 2021. Diverse meibum lipids produced by Awat1 and Awat2 are important
658 for stabilizing tear film and protecting the ocular surface. iScience 24:102478.
659 https://doi.org/10.1016/j.isci.2021.102478
660 43. Poulos A, Sharp P, Johnson D, Easton C. 1988. The occurrence of polyenoic very
661 long chain fatty acids with greater than 32 carbon atoms in molecular species of
662 phosphatidylcholine in normal and peroxisome-deficient (Zellweger's syndrome)
663 brain. Biochem J 253:645–650. https://doi.org/10.1042/bj2530645
664 44. Robinson BS, Johnson DW, Poulos A. 1990. Unique molecular species of
665 phosphatidylcholine containing very-long-chain (C24–C38) polyenoic fatty acids in
666 rat brain. Biochem J 265:763–767. https://doi.org/10.1042/bj2650763
667 45. Nie L, Pascoa TC, Pike ACW, Bushell SR, Quigley A, Ruda GF, Chu A, Cole V,
668 Speedman D, Moreira T, Shrestha L, Mukhopadhyay SMM, Burgess-Brown NA,
669 Love JD, Brennan PE, Carpenter EP. 2021. The structural basis of fatty acid

elongation by the ELOVL elongases. Nat Struct Mol Biol 28:512–520. https://doi.org/10.1038/s41594-021-00605-6

46. Mizutani Y, Sun H, Ohno Y, Sassa T, Wakashima T, Obara M, Yuyama K, Kihara A, Igarashi Y. 2013. Cooperative synthesis of ultra long-chain fatty acid and ceramide during keratinocyte differentiation. PLoS One 8:e67317. https://doi.org/10.1371/journal.pone.0067317

47. Yamamoto M, Sassa T, Kyono Y, Uemura H, Kugo M, Hayashi H, Imai Y, Yamanishi K, Kihara A. 2021. Comprehensive stratum corneum ceramide profiling reveals reduced acylceramides in ichthyosis patient with *CERS3* mutations. J Dermatol 48:447–456. https://doi.org/10.1111/1346-8138.15725

48. Kim M, Habiba A, Doherty JM, Mills JC, Mercer RW, Huettner JE. 2009. Regulation of mouse embryonic stem cell neural differentiation by retinoic acid. Dev Biol 328:456–471. https://doi.org/10.1016/j.ydbio.2009.02.001

49. Richardson CD, Ray GJ, DeWitt MA, Curie GL, Corn JE. 2016. Enhancing homology-directed genome editing by catalytically active and inactive CRISPR-Cas9 using asymmetric donor DNA. Nat Biotechnol 34:339–344. https://doi.org/10.1038/nbt.3481

50. Deák F, Anderson RE, Fessler JL, Sherry DM. 2019. Novel cellular functions of very long chain-fatty acids: insight from ELOVL4 mutations. Front Cell Neurosci 13:428. https://doi.org/10.3389/fncel.2019.00428

690 51. Yeboah GK, Lobanova ES, Brush RS, Agbaga MP. 2021. Very long chain fatty
691 acid-containing lipids: a decade of novel insights from the study of ELOVL4. J Lipid
692 Res 62:100030. https://doi.org/10.1016/j.jlr.2021.100030
693 52. Ikeda M, Kanao Y, Yamanaka M, Sakuraba H, Mizutani Y, Igarashi Y, Kihara A.
694 2008. Characterization of four mammalian 3-hydroxyacyl-CoA dehydratases
695 involved in very long-chain fatty acid synthesis. FEBS Lett 582:2435–2440.
696 https://doi.org/10.1016/j.febslet.2008.06.007
697 53. Borroni B, Di Gregorio E, Orsi L, Vaula G, Costanzi C, Tempia F, Mitro N, Caruso
698 D, Manes M, Pinessi L, Padovani A, Brusco A, Boccone L. 2016. Clinical and
699 neuroradiological features of spinocerebellar ataxia 38 (SCA38). Parkinsonism Relat
700 Disord 28:80–86. https://doi.org/10.1016/j.parkreldis.2016.04.030
701 54. Di Gregorio E, Borroni B, Giorgio E, Lacerenza D, Ferrero M, Lo Buono N, Ragusa
702 N, Mancini C, Gaussen M, Calcia A, Mitro N, Hoxha E, Mura I, Coviello DA, Moon
703 YA, Tesson C, Vaula G, Couarch P, Orsi L, Duregon E, Papotti MG, Deleuze JF,
704 Imbert J, Costanzi C, Padovani A, Giunti P, Maillet-Vioud M, Durr A, Brice A,
705 Tempia F, Funaro A, Boccone L, Caruso D, Stevanin G, Brusco A. 2014. *ELOVL5*
706 mutations cause spinocerebellar ataxia 38. Am J Hum Genet 95:209–217.
707 https://doi.org/10.1016/j.ajhg.2014.07.001
708 55. Gazulla J, Orduna-Hospital E, Benavente I, Rodríguez-Valle A, Osorio-Caicedo P,
709 Alvarez-de Andrés S, García-González E, Fraile-Rodrigo J, Fernández-Tirado FJ,

710 Berciano J. 2020. Contributions to the study of spinocerebellar ataxia type 38
711 (SCA38). J Neurol 267:2288–2295. https://doi.org/10.1007/s00415-020-09840-1
712 56. Jojima K, Edagawa M, Sawai M, Ohno Y, Kihara A. 2020. Biosynthesis of the
713 anti-lipid-microdomain sphingoid base 4,14-sphingadiene by the ceramide desaturase
714 FADS3. FASEB J 34:3318–3335. https://doi.org/10.1096/fj.201902645r
715 57. Kihara A, Anada Y, Igarashi Y. 2006. Mouse sphingosine kinase isoforms SPHK1a
716 and SPHK1b differ in enzymatic traits including stability, localization, modification,
717 and oligomerization. J Biol Chem 281:4532–4539.
718 https://doi.org/10.1074/jbc.m510308200
719 58. Ohno Y, Nakamichi S, Ohkuni A, Kamiyama N, Naoe A, Tsujimura H, Yokose U,
720 Sugiura K, Ishikawa J, Akiyama M, Kihara A. 2015. Essential role of the cytochrome
721 P450 CYP4F22 in the production of acylceramide, the key lipid for skin permeability
722 barrier formation. Proc Natl Acad Sci U S A 112:7707–7712.
723 https://doi.org/10.1073/pnas.1503491112
724 59. Ohno Y, Kamiyama N, Nakamichi S, Kihara A. 2017. PNPLA1 is a transacylase
725 essential for the generation of the skin barrier lipid ω-*O*-acylceramide. Nat Commun
726 8:14610. https://doi.org/10.1038/ncomms14610
727 60. Kitamura T, Takagi S, Naganuma T, Kihara A. 2015. Mouse aldehyde dehydrogenase
728 ALDH3B2 is localized to lipid droplets via two C-terminal tryptophan residues and
729 lipid modification. Biochem J 465:79–87. https://doi.org/10.1042/bj20140624

730 61. Kitamura T, Seki N, Kihara A. 2017. Phytosphingosine degradation pathway includes
731 fatty acid α-oxidation reactions in the endoplasmic reticulum. Proc Natl Acad Sci U S
732 A 114:E2616–E2623. https://doi.org/10.1073/pnas.1700138114
733

FIG 1 Multiple alignment of ELOVL1–7. Amino acid sequences of human ELOVL1–7 proteins were aligned using Clustal Omega (https://www.ebi.ac.uk/Tools/msa/clustalo/). The numbers in the right-hand margin refer to the adjacent amino acid residues. Amino acid residues conserved in all seven isozymes are indicated by black boxes, while residues conserved in five or six isozymes are indicated by gray boxes. SCA34-substituted residues in ELOVL4 and corresponding residues in ELOVL7 are indicated by cyan and orange boxes, respectively. The catalytically important histidine box is marked by a red rectangle.

FIG 2 Positions of the amino acid residues of ELOVL4 that are substituted in SCA34 mapped to the crystal structure of ELOVL7. Five amino acid residues of ELOVL4 that are substituted in SCA34 (magenta) mapped on the ribbon diagram of the human ELOVL7 structure with the bound acyl-CoA analog containing the C20:0 FA moiety (PDB: 6Y7F) (45). The catalytically important histidine box (H-box) is shown in lime green.

FIG 3 Localization of ELOVL4 SCA34 mutant proteins in the ER. HeLa cells were transfected with a vector or each of the *3×FLAG-ELOVL4*-encoding plasmids: WT and five SCA34 mutants (L168F, I171T, Q180P, T233M, and W246G). Twenty-four hours after transfection, the cells were fixed and subjected to indirect immunofluorescence microscopy

753 using anti-FLAG antibody (red) and anti-calnexin antibody (green), which mark the ER.
754 Nuclei were stained with DAPI (blue). Scale bar, 10 μm.
755
756 **FIG 4** Incomplete elongation of ULC PUFAs by ELOVL4 SCA34 mutants. (A)
757 Structures of a representative ULC PUFA-containing ceramide (upper) and ULC-PC
758 (lower): a ceramide that contains C32:6 FA (upper) and a PC that contains FAs (lower)
759 making a total of C50:7 (C32:6 FA in the *sn*-1 position plus C18:1 in the *sn*-2 position). (B)
760 Schematic representations of PUFA elongation pathways (n–6 and n–3 series). Linoleic
761 acid (C18:2n–6) and α-linolenic acid (C18:3n–3) are subject to a series of reactions,
762 including desaturation, elongation by ELOVL isozymes, and β-oxidation, and some of the
763 products are elongated to ULC PUFAs by ELOVL4. The letter E denotes ELOVL
764 isozymes and font size reflects the relative strength of their activities. (C–G) HEK 293T
765 cells were transfected with a vector or each of the *3×FLAG-ELOVL4*-encoding plasmids
766 (WT, L168F, I171T, Q180P, T233M, W246G, and R216X), together with
767 *3×FLAG-CERS3*- and *HA-ELOVL2*-encoding plasmids (C–E) or *HA-ELOVL2*-encoding
768 plasmid (F and G) for 48 h. (C and F) Total lysates prepared from the transfected cells were
769 separated by SDS-PAGE, followed by immunoblotting with anti-FLAG, anti-HA, and
770 anti-α-tubulin (for loading control) antibodies. (D, E, G) Lipids were extracted from the
771 transfected cells, and ceramides (D and E) or PCs (G) containing the indicated FA moiety
772 were analyzed by LC–MS/MS. PC species are expressed as the sum of the chain-length and

773 the number of double bonds of two constituent FAs. (D and G) Heatmaps presenting the
774 levels of ceramide (D) or PC (G) species in each kind of ELOVL4 mutant-expressing cell
775 relative to those in ELOVL4 WT-expressing cells (n = 3 independent cell cultures). (E)
776 Percentages of the C32:6 and C38:6 ceramides among the total ceramides quantified in (D).
777 Values represent means + SD (n = 3 independent cell cultures). Significant differences in
778 comparison to ELOVL4 WT-expressing cells (*P < 0.05; **P < 0.01; Dunnett's test) are
779 indicated.
780
781 **FIG 5** Differentiation of ES cells into neurons induces *Elovl4* expression and ULC-PC
782 production. ES cells were differentiated into neurons in neuronal differentiation medium for
783 5 days. The cells were harvested for RNA and lipid extractions prior to the initiation of
784 differentiation (day 0), on day 1, and on day 5. (A) On days 0, 1, and 5, bright-field images
785 of live cells were captured, then the cells were fixed and subjected to indirect
786 immunofluorescence microscopy using anti-class III β-tubulin antibody (green). Nuclei
787 were stained with DAPI (blue). Scale bars, 100 μm (day 0) and 25 μm (days 1 and 5). (B)
788 Total RNAs were prepared from the cells on days 0, 1, and 5, and were subjected to
789 real-time quantitative RT-PCR using specific primers for *Elovl4* or *Actb*. Values presented
790 are the mean (+ SD) levels of *Elovl4* mRNA relative to those of *Actb* (3 independent cell
791 cultures). (C) Lipids were extracted from the cells on days 0, 1, and 5, and ULC-PCs were

analyzed by LC–MS/MS. Values presented are mean (+ SD) levels of ULC-PCs (3 independent cell cultures).

FIG 6 Incomplete elongation of ULC PUFAs in *ELOVL4* Q180P and W246G KI neurons. (A) The gene structure of *Elovl4* and sequence chromatograms of the Q180P and W246G mutations in control, heterozygous Q180P, heterozygous W246G, and homozygous W246G KI ES cells. (B and C) Control and KI ES cells were differentiated into neurons for 1 (B) and 5 days (B and C). (B) Lipids were extracted and the PC species C44:5–C56:7, which are expressed according to the sum of their chain length and the number of double bonds in their two constituent FAs, were analyzed by LC–MS/MS. Values in the left panels on days 1 and 5 represent mean (+ SD) levels of PCs (3 independent cell cultures), with each PC species being color-coded. Values in the right panels on days 1 and 5 represent the percentages of ≥ C52 ULC-PCs among the sum of C44:5–C56:7 PCs (3 independent cell cultures). Significant differences from control cells (*$P < 0.05$; **$P < 0.01$; Dunnett's test) are indicated. (C) Total RNAs were prepared from the cells and subjected to real-time quantitative RT-PCR using specific primers for *Elovl2*, *Elovl4*, *Elovl5*, *Tubb3*, or *Actb*. Values presented are mean (+ SD) levels of each mRNA relative to those of *Actb* and expressed as a ratio to the control cells (3 independent cell cultures). Significant differences from control cells (*$P < 0.05$; **$P < 0.01$; Dunnett's test) are indicated. Het, heterozygous; Homo, homozygous.

FIG 7 Model for the dominant mode of inheritance in SCA34. One C24/C26 acyl-CoA synthesized by ELOVL5 and ELOVL2 is elongated by the same WT or SCA34 mutant ELOVL4 protein (black arrows). In normal cases, in which both *ELOVL4* alleles are WT, C24/C26 acyl-CoAs are elongated to become C34–C38; this process produces highly functional ULC-PCs. In patients with ISQMR, in whom both *ELOVL4* alleles are ISQMR mutants, C24/C26 acyl-CoAs cannot be elongated by the ISQMR mutant protein (gray arrows with crosses), and there is no production of ≥ C28 ULC-PCs. In ISQMR carriers, in whom one allele is WT and the other allele is an ISQMR mutant, all C24/C26 acyl-CoAs are elongated by the remaining WT protein; thus, normal levels of highly functional ULC-PCs may be produced. In patients with SCA34 in whom one allele is WT and the other allele is an SCA34 mutant, a proportion of C24/C26 acyl-CoAs are elongated normally to C34–C38 by the WT protein. The remaining proportion is elongated by the SCA34 protein only up to C32, thereby producing weakly functional ULC-PCs. Gray arrows indicate reduced elongation.

829 **TABLE 1** Oligonucleotides used for the generation of mutated *ELOVL4* plasmids.

Primer name	Sequence
ELOVL4_F	5'-GGATCCATGGGGCTCCTGGACTCGGAGCCGG-3' (*Bam*HI)
ELOVL4_R	5'-TTAATCTCCTTTTGCTTTTCCATTTTTC-3'
E4_L168F-1	5'-TGTTTACCTTCTGGTGGATTGGAATTAAGTG-3'
E4_L168F-2	5'-CAATCCACCAGAAGGTAAACATCGTACAGTG-3'
E4_I171T-1	5'-TTGTGGTGGACTGGAATTAAGTGGGTTGCAG-3'
E4_I171T-2	5'-CTTAATTCCAGTCCACCACAAGGTAAACATC-3'
E4_Q180P-1	5'-GCAGGAGGACCAGCATTTTTTGGAGCCCAGTTG-3'
E4_Q180P-2	5'-AAAAAATGCTGGTCCTCCTGCAACCCACTTAATTC-3'
E4_T233M-1	5'-ATTGGGCACATGGCACTGTCTCTTTACACTG-3'
E4_T233M-2	5'-AGACAGTGCCATGTGCCCAATGGTCACATGG-3'
E4_W246G-1	5'-CTTCCCCAAAGGGATGCACTGGGCTCTAATTG-3'
E4_W246G-2	5'-CAGTGCATCCCTTTGGGGAAGGGGCAGTCAG-3'
E4_R216X-1	5'-TTGGTGGAAATGATACCTGACTATGTTGCAAC-3'
E4_R216X-2	5'-GTCAGGTATCATTTCCACCAAAGATATTTCTG-3'

830 The restriction enzyme *Bam*HI used for cloning into the expression vector is noted in

831 parentheses, with its sequence underlined.

832 **TABLE 2** Oligonucleotides used for the generation of CRISPR/Cas9 plasmids.

Oligonucleotide name	Sequence	Plasmid name
mElovl4_Q180P-gRNA_F1	5’-GAAAGGTGGGTCCCTCACCTGTTTT-3’	pUKA27
mElovl4_Q180P-gRNA_R1	5’-AGGTGAGGGACCCACCTTTCCGGTG-3’	
mElovl4_W246G-gRNA_F1	5’-AGAGCCCAGTGCATCCACTTGTTTT-3’	pUKA16
mElovl4_W246G-gRNA_R1	5’-AAGTGGATGCACTGGGCTCTCGGTG-3’	

833

834 **TABLE 3** ssODNs used for homology-directed repair

Elovl4 mutation	Sequence
Q180P	5'-CTAGGTAAACCTACTCCCACCCACATGGGGGTTCAGAC AGAAAGGTGGGTCCCTCACCGGGCCCTCCAGCCACCCAC TTGATTCCAATCCACCACAGAGTGAACATGGTGCAGTGGT GGT-3' (*Apa*I)
W246G	5'-GTAGAAGTTGAGGAAGAGGAAGATGAAGCTGATGGCG TAGGCGATCAGAGCCCAGTGCATGCCCTTGGGGAAGGGG CAGTCGGTGTAGAGAGACAGTGCTGTGTGTCCGATGGTC ACGTGGAA-3' (*Sph*I)

835 The restriction enzymes used for genotyping KI cells are noted in parentheses, with their

836 sequences underlined.

837

838 **TABLE 4** Selected *m/z* values and collision energies for the detection of ceramide species

839 in the LC–MS/MS analysis.

Acyl chain	Precursor ions (Q1, *m/z*)		Product ion (Q3, *m/z*)	Collision energy (eV)
	$[M - H_2O + H]^+$	$[M + H]^+$		
C18:0	548.6	566.6	264.3	20
C20:0	576.6	594.6	264.3	20
C22:0	604.6	622.6	264.3	25
C24:0	632.6	650.6	264.3	30
C26:0	660.7	678.7	264.3	30
C28:0	688.7	706.7	264.3	30
C30:0	716.7	734.7	264.3	35
C32:0	744.8	762.8	264.3	40
C34:0	772.8	790.8	264.3	40
C18:1	546.6	564.6	264.3	20
C20:1	574.6	592.6	264.3	20
C22:1	602.6	620.6	264.3	25
C24:1	630.6	648.6	264.3	30
C26:1	658.7	676.7	264.3	30
C28:1	686.7	704.7	264.3	30
C30:1	714.7	732.7	264.3	35
C32:1	742.8	760.8	264.3	35
C34:1	770.8	788.8	264.3	40
C36:1	798.8	816.8	264.3	40
C38:1	826.8	844.8	264.3	40
C24:4	624.6	642.6	264.3	30
C26:4	652.7	670.7	264.3	30

C28:4	680.7	698.7	264.3	30
C30:4	708.7	726.7	264.3	35
C32:4	736.8	754.8	264.3	35
C34:4	764.8	782.8	264.3	40
C36:4	792.8	810.8	264.3	40
C38:4	820.9	838.9	264.3	40
C30:5	706.7	724.7	264.3	35
C32:5	734.7	752.7	264.3	35
C34:5	762.8	780.8	264.3	40
C36:5	790.8	808.8	264.3	40
C38:5	818.8	836.8	264.3	40
C30:6	704.7	722.7	264.3	35
C32:6	732.7	750.7	264.3	35
C34:6	760.8	778.8	264.3	40
C36:6	788.8	806.8	264.3	40
C38:6	816.8	834.8	264.3	40

840

841 **TABLE 5** Selected *m/z* values for the detection of PC species in the LC–MS/MS analysis.

Sum of two acyl chains	Precursor ion (Q1, *m/z*)	Product ion (Q3, *m/z*)
C33:1-d_7	753.5	184.0
C44:5	892.8	184.0
C44:6	890.8	184.0
C44:7	888.7	184.0
C46:5	920.8	184.0
C46:6	918.8	184.0
C46:7	916.8	184.0
C48:5	948.8	184.0
C48:6	946.8	184.0
C48:7	944.8	184.0
C50:5	976.9	184.0
C50:6	974.9	184.0
C50:7	972.8	184.0
C52:5	1004.9	184.0
C52:6	1002.9	184.0
C52:7	1000.9	184.0
C54:5	1032.9	184.0
C54:6	1030.9	184.0
C54:7	1028.9	184.0
C56:5	1061.0	184.0
C56:6	1059.0	184.0
C56:7	1056.9	184.0

842 Collision energy and cone voltage were 30 eV and 15 V, respectively.

843

844 **TABLE 6** Primers used for real-time quantitative RT-PCR.

Primer name	Sequence
mElovl4-rt_F1	5’-ACGTGATCATGTACTCCTACTATGG-3’
mElovl4-rt_R1	5’-CCGTTCGATGAGATACCATTCGTGG-3’
mTubb3-rt_F3	5’-GAGGCCTCCTCTCACAAGTATGTGC-3’
mTubb3-rt_R3	5’-GTTGCCAGCACCACTCTGACCAAAG-3’
mElovl2-rt_F	5’-GCTGGTCATCCTGTTCTTAAACTTC-3’
mElovl2-rt_R	5’-TTATTGAGCCTTCTTGTCCGTCATG-3’
mElovl5-rt_F2	5’-TCGGGTGGCTGTTCTTCCAGATTGG-3’
mElovl5-rt_R	5’-AGGGAAGCTGTTGGTGTGTCCGTTG-3’
Mouse_Actb_primer	Mouse Housekeeping Gene Primer Set (Takara Bio)

845

Fig. 1

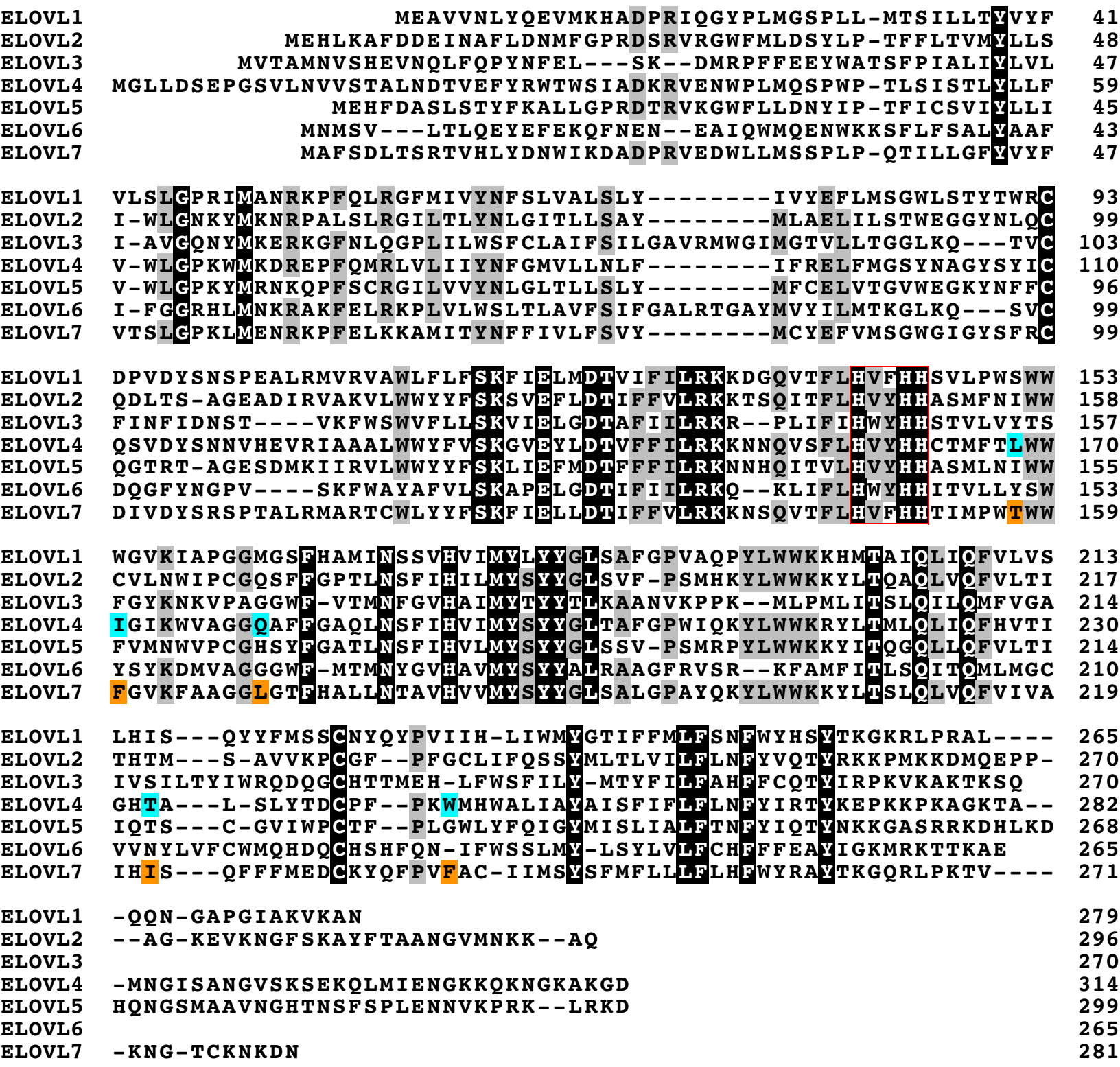

ELOVL1 MEAVVNLYQEVMKHADPRIQGYPLMGSPLL-MTSILLTYVYF 41
ELOVL2 MEHLKAFDDEINAFLDNMFGPRDSRVRGWFMLDSYLP-TFFLTVMYLLS 48
ELOVL3 MVTAMNVSHEVNQLFQPYNFEL---SK--DMRPFFEEYWATSFPIALIYLVL 47
ELOVL4 MGLLDSEPGSVLNVVSTALNDTVEFYRWTWSIADKRVENWPLMQSPWP-TLSISTLYLLF 59
ELOVL5 MEHFDASLSTYFKALLGPRDTRVKGWFLLDNYIP-TFICSVIYLLI 45
ELOVL6 MNMSV---LTLQEYEFEKQFNEN--EAIQWMQENWKKSFLFSALYAAF 43
ELOVL7 MAFSDLTSRTVHLYDNWIKDADPRVEDWLLMSSPLP-QTILLGFYVYF 47
ELOVL1 VLSLGPRIMANRKPFQLRGFMIVYNFSLVALSLY--------IVYEFLMSGWLSTYTWRC 93
ELOVL2 I-WLGNKYMKNRPALSLRGILTLYNLGITLLSAY--------MLAELILSTWEGGYNLQC 99
ELOVL3 I-AVGQNYMKERKGFNLQGPLILWSFCLAIFSILGAVRMWGIMGTVLLTGGLKQ---TVC 103
ELOVL4 V-WLGPKWMKDREPFQMRLVLIIYNFGMVLLNLF--------IFRELFMGSYNAGYSYIC 110
ELOVL5 V-WLGPKYMRNKQPFSCRGILVVYNLGLTLLSLY--------MFCELVTGVWEGKYNFFC 96
ELOVL6 I-FGGRHLMNKRAKFELRKPLVLWSLTLAVFSIFGALRTGAYMVYILMTKGLKQ---SVC 99
ELOVL7 VTSLGPKLMENRKPFELKKAMITYNFFIVLFSVY--------MCYEFVMSGWGIGYSFRC 99
ELOVL1 DPVDYSNSPEALRMVRVAWLFLFSKFIELMDTVIFILRKKDGQVTFLHVFHHSVLPWSWW 153
ELOVL2 QDLTS-AGEADIRVAKVLWWYYFSKSVEFLDTIFFVLRKKTSQITFLHVYHHASMFNIWW 158
ELOVL3 FINFIDNST----VKFWSWVFLLSKVIELGDTAFIILRKR--PLIFIHWYHHSTVLVYTS 157
ELOVL4 QSVDYSNNVHEVRIAAALWWYFVSKGVEYLDTVFFILRKKNNQVSFLHVYHHCTMFTLWW 170
ELOVL5 QGTRT-AGESDMKIIRVLWWYYFSKLIEFMDTFFFILRKNNHQITVLHVYHHASMLNIWW 155
ELOVL6 DQGFYNGPV----SKFWAYAFVLSKAPELGDTIFIILRKQ--KLIFLHWYHHITVLLYSW 153
ELOVL7 DIVDYSRSPTALRMARTCWLYYFSKFIELLDTIFFVLRKKNSQVTFLHVFHHTIMPWTWW 159
ELOVL1 WGVKIAPGGMGSFHAMINSSVHVIMYLYYGLSAFGPVAQPYLWWKKHMTAIQLIQFVLVS 213
ELOVL2 CVLNWIPCGQSFFGPTLNSFIHILMYSYYGLSVF-PSMHKYLWWKKYLTQAQLVQFVLTI 217
ELOVL3 FGYKNKVPAGGWF-VTMNFGVHAIMYTYYTLKAANVKPPK--MLPMLITSLQILQMFVGA 214
ELOVL4 IGIKWVAGGQAFFGAQLNSFIHVIMYSYYGLTAFGPWIQKYLWWKRYLTMLQLIQFHVTI 230
ELOVL5 FVMNWVPCGHSYFGATLNSFIHVLMYSYYGLSSV-PSMRPYLWWKKYITQGQLLQFVLTI 214
ELOVL6 YSYKDMVAGGGWF-MTMNYGVHAVMYSYYALRAAGFRVSR--KFAMFITLSQITQMLMGC 210
ELOVL7 FGVKFAAGGLGTFHALLNTAVHVVMYSYYGLSALGPAYQKYLWWKKYLTSLQLVQFVIVA 219
ELOVL1 LHIS---QYYFMSSCNYQYPVIIH-LIWMYGTIFFMLFSNFWYHSYTKGKRLPRAL---- 265
ELOVL2 THTM---S-AVVKPCGF--PFGCLIFQSSYMLTLVILFLNFYYVQTYRKKPMKKDMQEPP- 270
ELOVL3 IVSILTYIWRQDQGCHTTMEH-LFWSFILY-MTYFILFAHFFCQTYIRPKVKAKTKSQ 270
ELOVL4 GHTA---L-SLYTDCPF--PKWMHWALIAYAISFIFLFLNFYIRTYKEPKKPKAGKTA-- 282
ELOVL5 IQTS---C-GVIWPCTF--PLGWLYFQIGYMISLIALFTNFYIQTYNKKGASRRKDHLKD 268
ELOVL6 VVNYLVFCWMQHDQCHSHFQN-IFWSSLMY-LSYLVLFCHFFFEAYIGKMRKTTKAE 265
ELOVL7 IHIS---QFFFMEDCKYQFPVFAC-IIMSYSFMFLLLFLHFWYRAYTKGQRLPKTV---- 271
ELOVL1 -QQN-GAPGIAKVKAN 279
ELOVL2 --AG-KEVKNGFSKAYFTAANGVMNKK--AQ 296
ELOVL3 270
ELOVL4 -MNGISANGVSKSEKQLMIENGKKQKNGKAKGD 314
ELOVL5 HQNGSMAAVNGHTNSFSPLENNVKPRK--LRKD 299
ELOVL6 265
ELOVL7 -KNG-TCKNKDN 281

Fig. 2

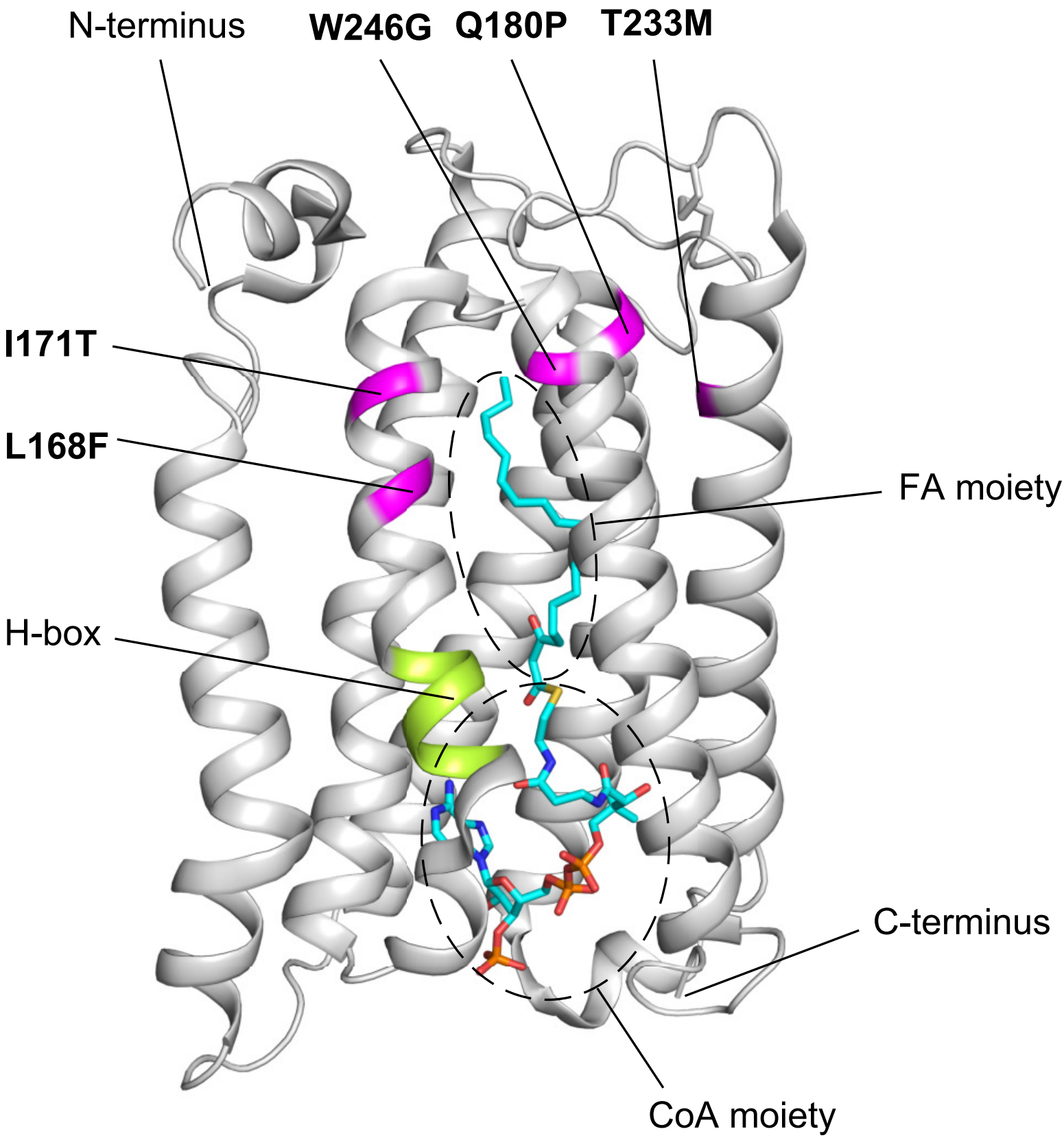

N-terminus
W246G
Q180P
T233M
I171T
L168F
FA moiety
H-box
C-terminus
CoA moiety

Fig. 3

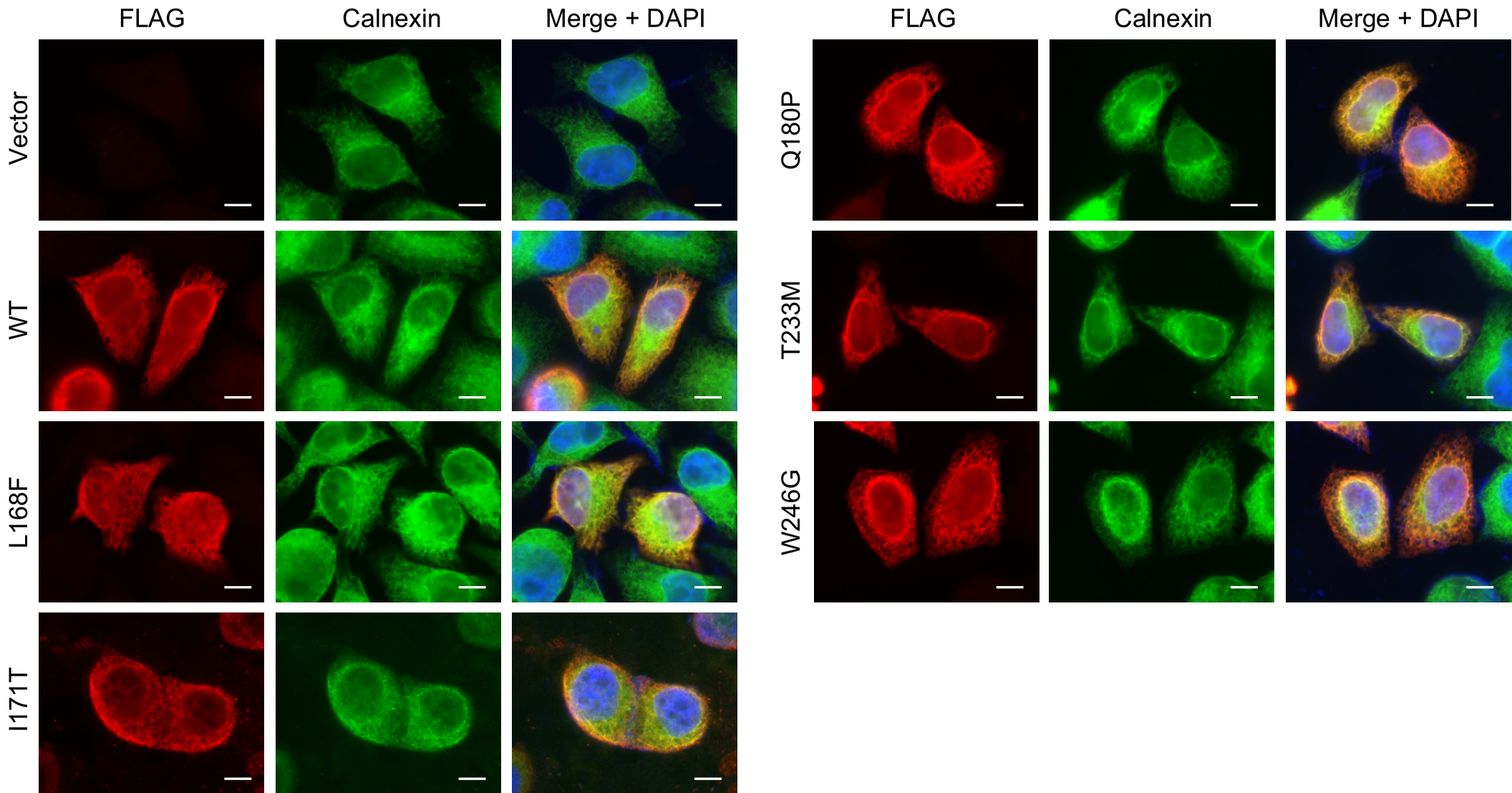

FLAG
Calnexin
Merge + DAPI
Vector
WT
L168F
I171T
FLAG
Calnexin
Merge + DAPI
Q180P
T233M
W246G

Fig. 4

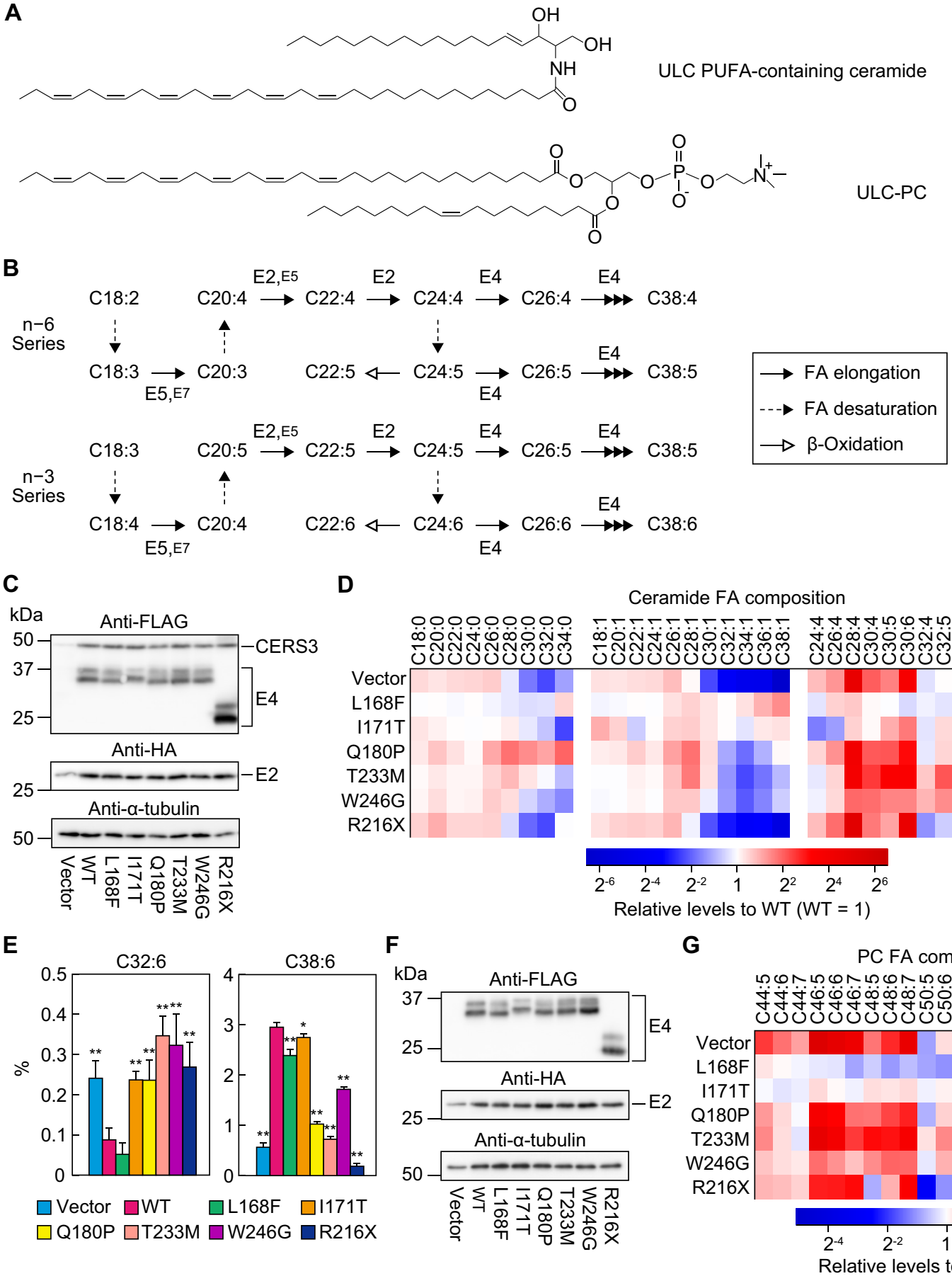
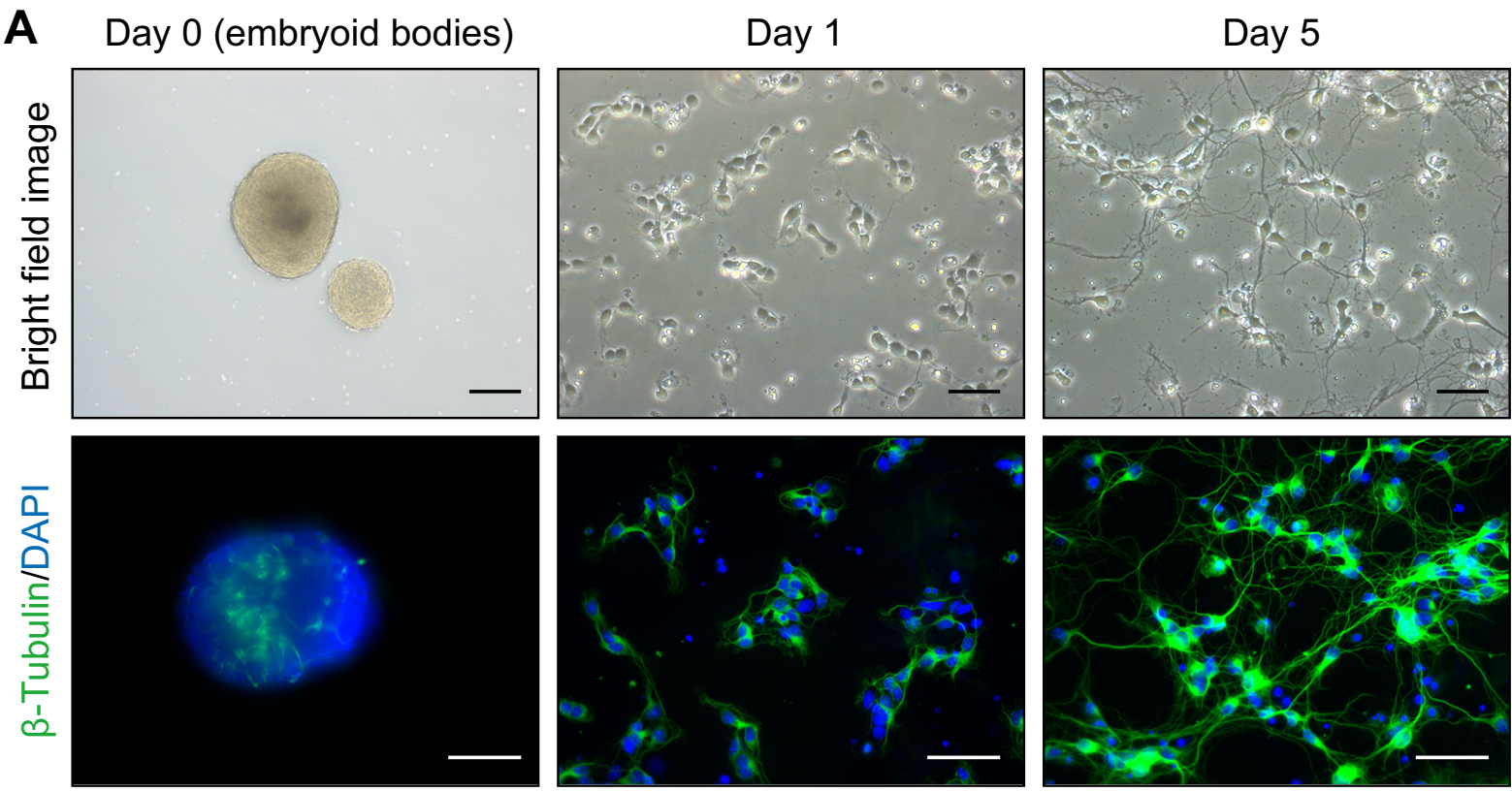
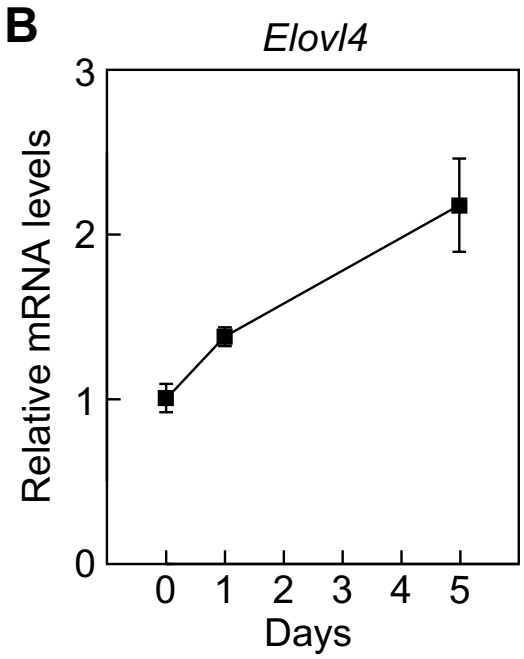

A
ULC PUFA-containing ceramide
ULC-PC
B
n−6 Series
n−3 Series
C18:2
C20:4
C22:4
C24:4
C26:4
C38:4
C18:3
C20:3
C22:5
C24:5
C26:5
C38:5
C18:4
C20:4
C22:6
C24:6
C26:6
C38:6
E2,E5
E2
E4
E5,E7
FA elongation
FA desaturation
β-Oxidation
C
kDa
Anti-FLAG
CERS3
E4
Anti-HA
E2
Anti-α-tubulin
Vector
WT
L168F
I171T
Q180P
T233M
W246G
R216X
D
Ceramide FA composition
Relative levels to WT (WT = 1)
E
C32:6
C38:6
%
F
kDa
Anti-FLAG
E4
Anti-HA
E2
Anti-α-tubulin
G
PC FA composition
Relative levels to WT (WT = 1)

Fig. 5


A
Day 0 (embryoid bodies)
Day 1
Day 5
Bright field image
β-Tubulin/DAPI


B
Elovl4
Relative mRNA levels
0
1
2
3
0 1 2 3 4 5
Days

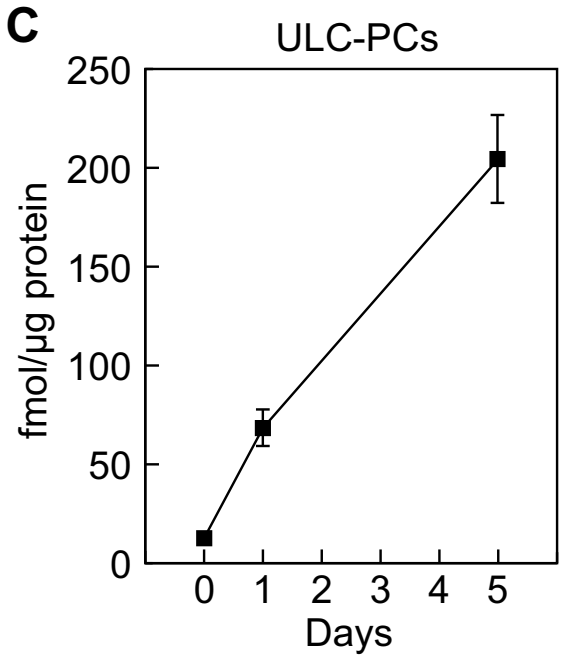

C
ULC-PCs
fmol/μg protein
0
50
100
150
200
250
0 1 2 3 4 5
Days

Fig. 6

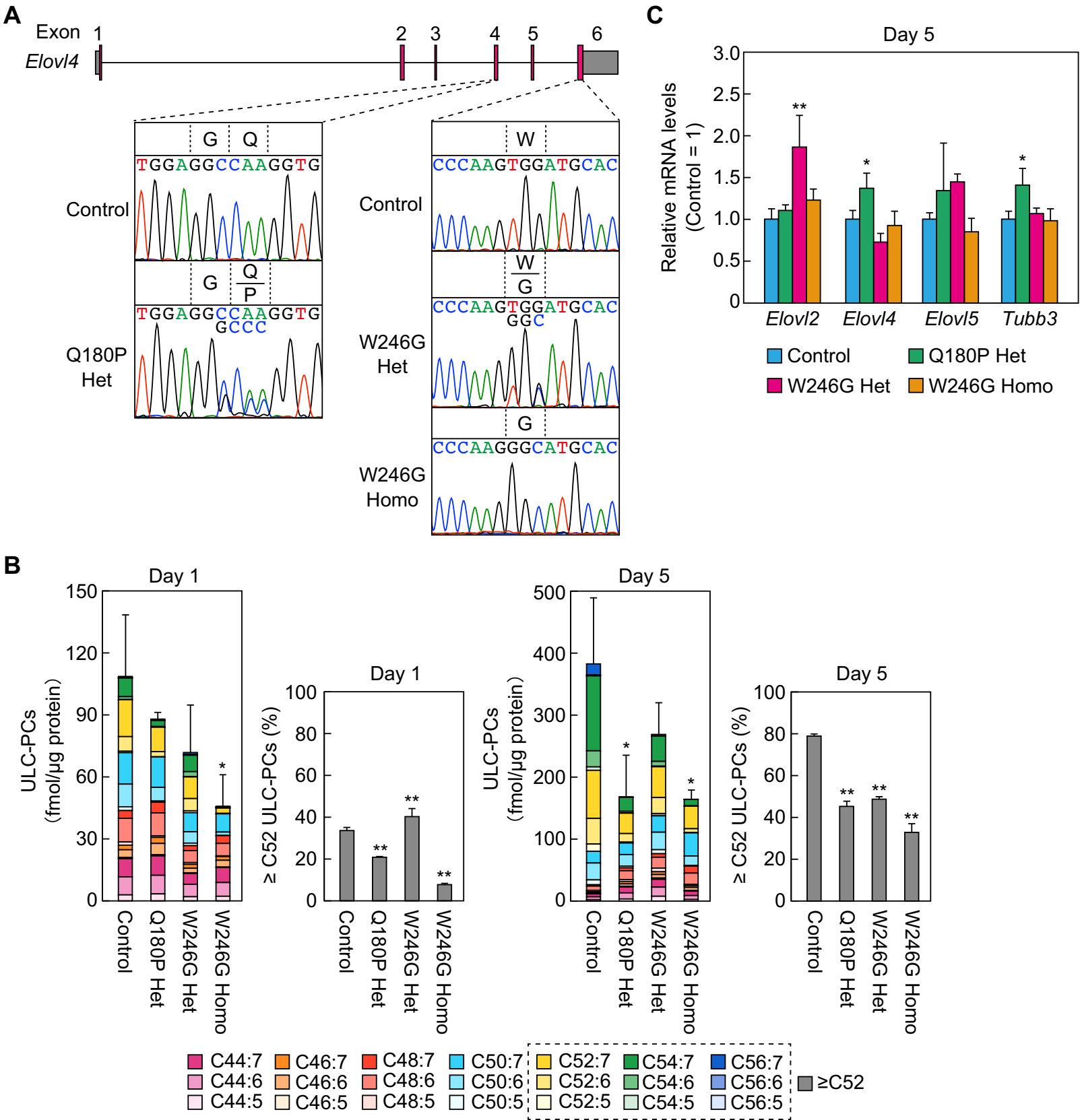
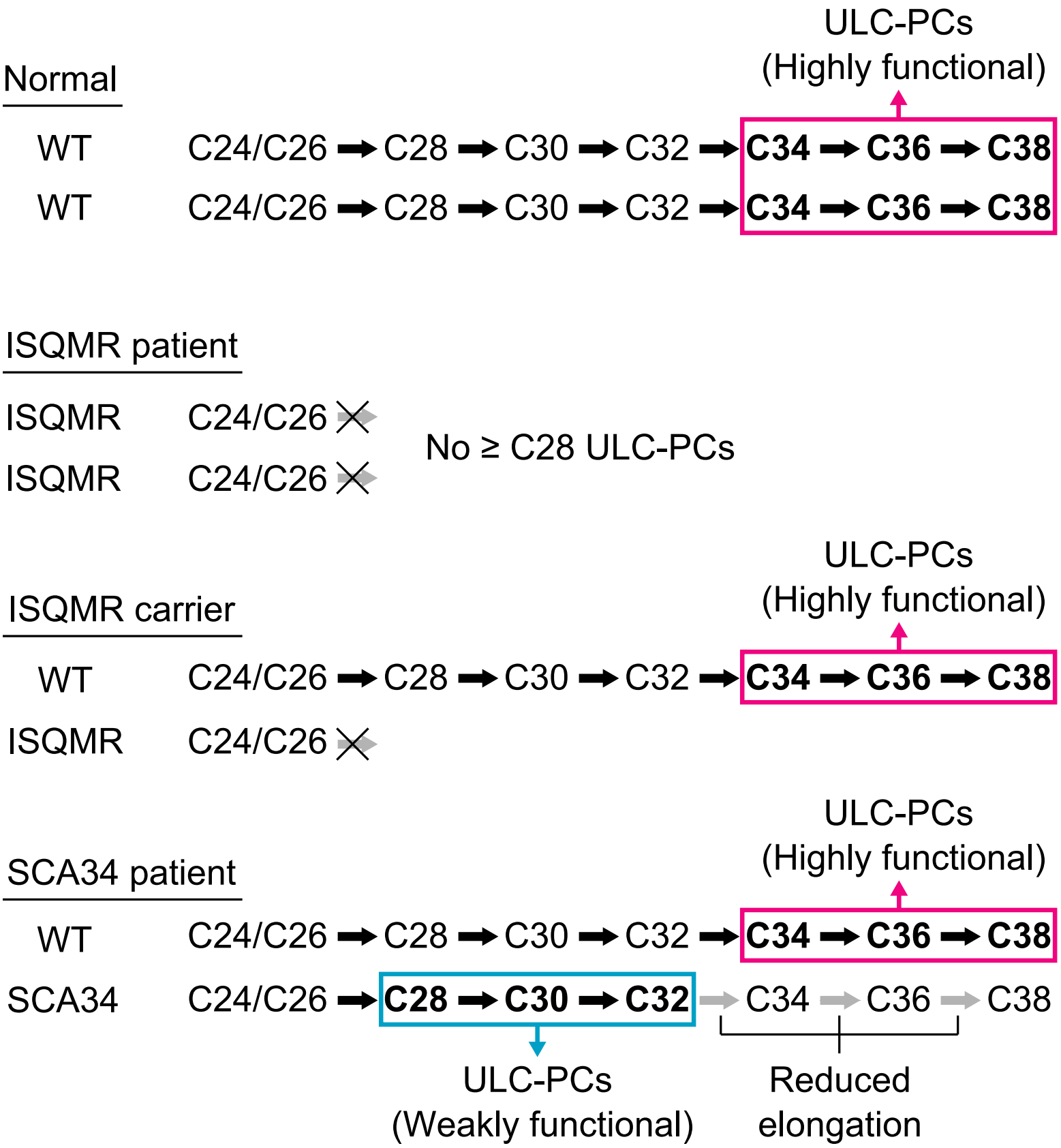

A
Exon 1 2 3 4 5 6
Elovl4
G Q
TGGAGGCCAAGGTG
Control
G Q/P
TGGAGGCCAAGGTG
GCCC
Q180P Het
W
CCCAAGTGGATGCAC
Control
W/G
CCCAAGTGGATGCAC
GGC
W246G Het
G
CCCAAGGGCATGCAC
W246G Homo
C
Day 5
Relative mRNA levels (Control = 1)
3.0
2.5
2.0
1.5
1.0
0.5
0
Elovl2 Elovl4 Elovl5 Tubb3
Control
Q180P Het
W246G Het
W246G Homo
B
Day 1
ULC-PCs (fmol/μg protein)
150
120
90
60
30
0
Control Q180P Het W246G Het W246G Homo
Day 1
≥ C52 ULC-PCs (%)
100
80
60
40
20
0
Control Q180P Het W246G Het W246G Homo
Day 5
ULC-PCs (fmol/μg protein)
500
400
300
200
100
0
Control Q180P Het W246G Het W246G Homo
Day 5
≥ C52 ULC-PCs (%)
100
80
60
40
20
0
Control Q180P Het W246G Het W246G Homo
C44:7 C46:7 C48:7 C50:7 C52:7 C54:7 C56:7
C44:6 C46:6 C48:6 C50:6 C52:6 C54:6 C56:6
C44:5 C46:5 C48:5 C50:5 C52:5 C54:5 C56:5
≥C52

Fig. 7


ULC-PCs
(Highly functional)
Normal
WT C24/C26 → C28 → C30 → C32 → C34 → C36 → C38
WT C24/C26 → C28 → C30 → C32 → C34 → C36 → C38
ISQMR patient
ISQMR C24/C26
ISQMR C24/C26
No ≥ C28 ULC-PCs
ISQMR carrier
ULC-PCs
(Highly functional)
WT C24/C26 → C28 → C30 → C32 → C34 → C36 → C38
ISQMR C24/C26
SCA34 patient
ULC-PCs
(Highly functional)
WT C24/C26 → C28 → C30 → C32 → C34 → C36 → C38
SCA34 C24/C26 → C28 → C30 → C32 → C34 → C36 → C38
ULC-PCs
(Weakly functional)
Reduced
elongation